Nonlinear vibration of multilayer shell-type structural elements with double curvature consisting of CNT patterned layers within different theories

M. Avey [a,*], N. Fantuzzi [b], A.H. Sofiyev [c], N. Kuruoglu [d]

[a] *Division of Mathematics in Graduate School of Natural and Applied Sciences of Usak University, Usak, Turkey*
[b] *Department of Civil, Chemical, Environmental, and Materials Engineering, University Bologna, Italy*
[c] *Department of Civil Engineering of Engineering Faculty of Suleyman, Demirel University, Isparta, Turkey*
[d] *Department of Civil Engineering of Faculty of Engineering and Architecture, Istanbul Gelisim University, Istanbul, Turkey*

ARTICLE INFO

ABSTRACT

In this article, the nonlinear vibration of moderately thick multilayer shell-type structural elements with double curvature consisting of carbon nanotube (CNT) patterned layers is investigated within different shell theories. The first order shear deformation theory has been generalized on the motion for moderately thick multilayer shell-type structural elements with double curvature consisting of CNT patterned layers for the first time. Then, by applying Galerkin and semi-inverse perturbation methods to motion equations, and the frequency-amplitude relationship is obtained. From these formulas, the expressions for nonlinear frequencies of multilayer spherical and hyperbolic-paraboloid shells, rectangular plate and cylindrical panels patterned by CNTs within shear deformation and classical shell theories are obtained in special cases. The reliability of obtained results is verified by comparison with other results reported in the literature. The effects of transverse shear strains, volume fraction, sequence and number of nanocomposite layers on nonlinear frequency are discussed in detail.

1. Introduction

Composite multilayer plates, panels and shells are one of basic structural components and are often used in a variety of engineering applications such as defense, aviation, turbo-machinery and shipbuilding industries. The wide range of applications of multilayer shell-type structural elements has led researchers to examine the performance of such structural components made of different materials and exposed to various dynamic loads for many years. In multilayer shell-type structural elements, the formation of deflections measurable with their own thickness requires the use of nonlinear shell theories. Studies on the geometrically nonlinear dynamic behavior of multilayer shells within shear deformation theory (SDT) began to emerge in the early 1960s [1]. The effect of transverse shear deformations on nonlinear vibrations of moderately thick multilayer shell-type members and their response analysis has also been the subject of research in many earlier studies [2–4]. In the above studies, it was stated that the influence of transverse shear deformations on nonlinear vibrations of multilayer shells is significant and needs to be taken into account. A systematic presentation of various problems of the nonlinear dynamics of multilayer plates and shells within different theories was carried out in

the book of Reddy [5]. Later, various studies of the theoretical and experimental results obtained on the nonlinear vibrations of moderately thick multilayer shells within SDTs have been carried on until today [6–15].

One of the most important manifestations of the acceleration of scientific and technological progress is associated primarily with the need to create new progressive composite materials. In most cases, this improvement is possible by reinforcing structural homogeneous composite materials with nanoscale materials that are much smaller than their size. In recent years, CNTs have been the most interesting and thoroughly studied nanoscale materials among new generation composite materials. CNTs were experimentally discovered in 1991 by the Japanese materials scientist Iijima in the production of fullerene by evaporation of an arc discharge [16]. The excellent mechanical, electrical, chemical, magnetic and other properties of CNTs lead to the use of polymer composites reinforced by them in various fields of technology [17]. Since research on composites reinforced by CNTs is very important for modern technology, it has always been the focus of researchers [18,19].

The increase of vibration amplitude, causing unexpected failures in nano-composite structural elements motivated mathematics and

engineers to pay more attention in solving nonlinear vibration problems of structural elements widely used in new industries. One of the first attempts at mathematical modeling and solution of nonlinear vibration of monolayer composite structural elements reinforced by CNTs is the study of Shen and Xiang [20]. In this study, a model of single-layer composite cylindrical shells containing CNT is created and the scientific infrastructure is built to solve various vibration and stability problems. After this research, some studies were carried out to solve the vibration problems of single-layer shells reinforced by CNTs [21–27].

Considering the geometric nonlinearity in the vibration problems of the multilayer structural elements consisting of CNT patterned layers creates significant qualitative and quantitative changes in the dynamic properties, complicates the derivation and solution of the basic equations as well as makes the analysis and interpretation more complex. These difficulties have limited the number of scientific studies on multilayer structural elements consisting of CNT patterned layers, and therefore very little work has been done on this subject today. These publications are devoted to the linear behavior of laminated composite plates consisting of CNT patterned layers within SDTs [28,29]. In addition to these publications, some important studies on the nonlinear vibration of mono and multi-layer shallow shells made of functionally graded materials should be highlighted [30–37].

A comprehensive review of the literature by the authors revealed that the problem of nonlinear vibrations of thin and moderately thick multilayer shell-type structural elements with double curvature consisting of CNT patterned layers has not been studied to date, and the study under discussion is devoted to solving this problem within the framework of different theories.

2. Formulation of the problem

2.1. Description of model

The multilayer shell-type structure with double curvature consisting of CNT patterned layers with side lengths a_1 and a_2, curvature radii r_1 and r_2, and total thickness h is shown in Fig. 1. It is assumed that the multilayer shell with double curvature is moderately thick, composed of CNT patterned nanocomposite layers of equal thickness (δ) and consists of N layers. The layers of the shell-type structure with double curvature consisting of CNT patterned nanocomposites are perfectly bonded to each other, they do not slip, and all layers remain elastic during deformation. The main axes of elasticity of each lamina are assumed to be parallel to the coordinate axes on the reference surface. The curvilinear coordinate system $x_1 x_2 x_3$ is located on the reference surface and left corner of the shell with double curvature; where x_1 and x_2 axes are on the reference surface $x_3 = 0$ and the x_3 axis is in the normal direction to the reference surface and is directed inward. The reference surface $x_3 = 0$ is located at the interface of the layers for even values of N, while the reference surface for the odd values of N is located in the mid-surface of the middle lamina.

2.2. Material properties of multilayer shell-type structural elements

The effective material properties of each lamina with various CNT patterns, based on the expanded rule of the mixture are expressed as follows [20]:

$$E_{11}^{(k)} = \eta_1^{(k)} V_{cn}^{(k)} E_{11cn}^{(k)} + V_m^{(k)} E_m^{(k)}, \quad E_{22}^{(k)} = \frac{\eta_2^{(k)} E_m^{(k)} E_{22cn}^{(k)}}{E_{22cn}^{(k)} V_m^{(k)} + E_m^{(k)} V_{cn}^{(k)}}, \quad G_{12}^{(k)} = \frac{\eta_3^{(k)} G_m^{(k)} G_{12cn}^{(k)}}{G_{12cn}^{(k)} V_m^{(k)} + G_m^{(k)} V_{cn}^{(k)}}$$

$$G_{12}^{(k)} = G_{13}^{(k)} = G_{23}^{(k)}, \nu_{12}^{(k)} = V_{cn}^{*(k)} \nu_{12cn}^{(k)} + V_m^{(k)} \nu_m^{(k)}, \quad \rho_t^{(k)} = V_{cn}^{(k)} \rho_{cn}^{(k)} + V_m^{(k)} \rho_m^{(k)}, \quad \bar{z} = z/h \tag{1}$$

where $E_m^{(k)}, G_m^{(k)}, \rho_m^{(k)}, \nu_m^{(k)}$ are the elasticity modulus, density and Poisson's ratio in the lamina k^{th}, and $E_{ijcn}^{(k)}, G_{ijcn}^{(k)}, \rho_{cn}^{(k)}, \nu_{12cn}^{(k)} (i,j = 1,2,3)$ are the corresponding mechanical properties for the pattering CNT phase in the lamina k^{th}, respectively, $\eta_i^{(k)} (i = 1, 2, 3)$ are the efficiency parameters in the lamina k^{th}. Here $V_{cn}^{(k)}$ and $V_m^{(k)}$ are the volume fraction (VF) of CNTs and lamina k^{th}, that obey the rule of $V_{cn}^{(k)} + V_m^{(k)} = 1$. The estimation of total VF of CNTs are expressed as:

$$V_{cn}^{*(k)} = \frac{M_{cn}^{(k)}}{M_{cn}^{(k)} + (\rho_{cn}^{(k)}/\rho_m^{(k)})(1 - M_{cn}^{(k)})} \tag{2}$$

where $M_{cn}^{(k)}$ is the mass fraction of CNTs.

The pattern of the VF for CNTs over the thickness of lamina k^{th} as uniform pattern (U) and three types of linear functions is shown in Fig. 2.

$$V_{cn}^{(k)} = \begin{cases} U & \text{at} \quad V_{cn}^{*(k)} \\ V & \text{at} \quad 2(0.5 - \bar{x}_3) V_{cn}^{*(k)} \\ O & \text{at} \quad 2(0.5 + \bar{x}_3) V_{cn}^{*(k)} \\ X & \text{at} \quad 4|\bar{x}_3| V_{cn}^{*(k)} \end{cases} \tag{3}$$

3. Basic equations

3.1. Constitutive equations

The constitutive relations for lamina k^{th} patterned by CNTs in multilayer shell-type structural elements within first order shear deformation theory (FSDT) can be expressed by the following form [10,36]:
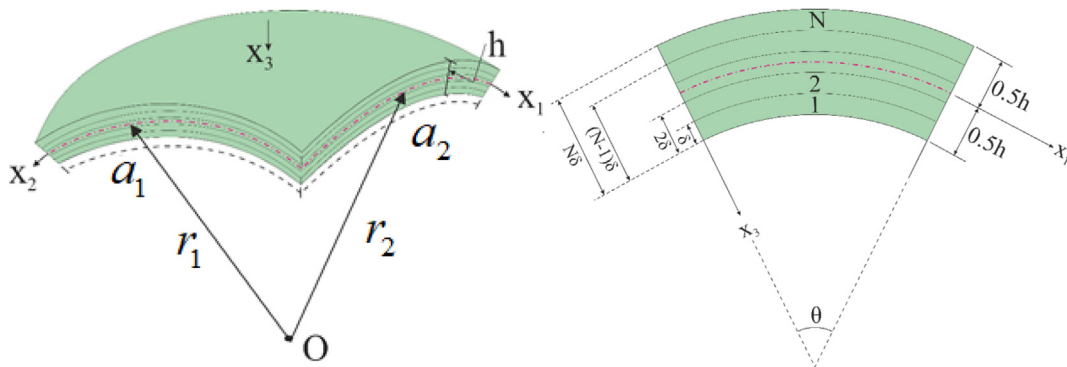

Fig. 1. (a) Multilayer shell-type structural elements with double curvature consisting of CNT patterned layers and (b) cross-section.
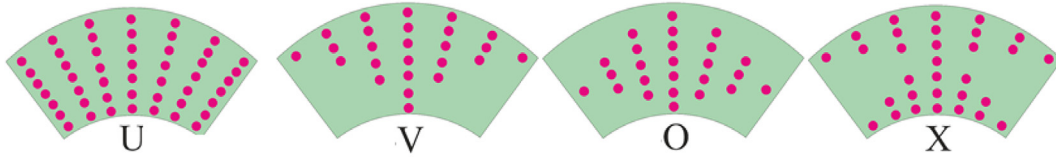
Fig. 2. Patterns of the VF for CNTs over the thickness of lamina k^{th}.

$$
\begin{bmatrix}
\sigma_{11}^{(k)} \\
\sigma_{22}^{(k)} \\
\sigma_{12}^{(k)} \\
\sigma_{13}^{(k)} \\
\sigma_{23}^{(k)}
\end{bmatrix}
=
\begin{bmatrix}
Q_{11\bar{x}_3}^{(k)} & Q_{12\bar{x}_3}^{(k)} & 0 & 0 & 0 \\
Q_{21\bar{x}_3}^{(k)} & Q_{22\bar{x}_3}^{(k)} & 0 & 0 & 0 \\
0 & 0 & Q_{66\bar{x}_3}^{(k)} & 0 & 0 \\
0 & 0 & 0 & Q_{55\bar{x}_3}^{(k)} & 0 \\
0 & 0 & 0 & 0 & Q_{44\bar{x}_3}^{(k)}
\end{bmatrix}
\begin{bmatrix}
e_{11} \\
e_{22} \\
e_{12} \\
e_{13} \\
e_{23}
\end{bmatrix}
\tag{4}
$$

where $\sigma_{ij}^{(k)}(i=1,2;j=1,2,3)$ denote the stresses in the lamina k^{th}, $e_{ij}(i,j=1,2,3)$ denote the strains and $Q_{ij\bar{x}_3}^{(k)}$, $(i,j=1,2,6)$, denote material properties of CNT patterned lamina k^{th} and expressed as:

$$
Q_{11\bar{x}_3}^{(k)} = \frac{E_{11}^{(k)}}{1-\nu_{12}^{(k)}\nu_{21}^{(k)}}, \quad Q_{22\bar{x}_3}^{(k)} = \frac{E_{22}^{(k)}}{1-\nu_{12}^{(k)}\nu_{21}^{(k)}}, Q_{12\bar{x}_3}^{(k)} = \nu_{21}^{(k)}Q_{11\bar{x}_3}^{(k)} = \nu_{12}^{(k)}Q_{22\bar{x}_3}^{(k)} = Q_{21\bar{x}_3}^{(k)},
$$
$$
Q_{44\bar{x}_3}^{(k)} = G_{23\bar{x}_3}^{(k)}, \quad Q_{55\bar{x}_3}^{(k)} = G_{13\bar{x}_3}^{(k)}, \quad Q_{66\bar{x}_3}^{(k)} = G_{12\bar{x}_3}^{(k)}.
\tag{5}
$$

in which $-\frac{h}{2} + \frac{(k-1)h}{N} \leqslant z \leqslant -\frac{h}{2} + \frac{kh}{N}$, $k = 1,2,...,N$, in which N is the number of lamina, $E_{ii}^{(k)}$, $G_{ij}^{(k)}(i,j=1,2,3)$ are Young and shear moduli of CNT patterned materials in the lamina k^{th}, $\nu_{12}^{(k)}$ and $\nu_{21}^{(k)}$ are Poisson ratios in the lamina k^{th} that are not dependent on location and satisfied the following equation $E_{22}^{(k)}\nu_{12}^{(k)} = E_{11}^{(k)}\nu_{21}^{(k)}$.

The shear stresses $\sigma_{j3}^{(k)}$ $(j=1,2)$ in the lamina k^{th} are expressed as [1]:

$$
\sigma_{j3}^{(k)} = \frac{df_j^{(k)}(x_3)}{dx_3}\psi_j(x_1, x_2, \tau), \quad (j=1,2)
\tag{6}
$$

where $\psi_j(x_1, x_2, \tau)$, $(j=1,2)$ are functions of rotation angles, $f_{jx_3}^{(k)}$ are shear stress functions in the lamina k^{th} and τ is a time.

3.2. Kinematic relations

Based on the Donnell-Mushtary type nonlinear shell theory and using relations (4), the strain components of any point not on the mid-surface of multilayer shell-type structural elements with double curvature consisting of CNT patterned layers can be expressed as follows:

$$
\begin{bmatrix}
e_{11} \\
e_{22} \\
e_{12}
\end{bmatrix}
=
\begin{bmatrix}
e_{11}^0 - x_3\frac{\partial^2 u_3}{\partial x_1^2} + I_{1x_3}^{(k)}\frac{\partial\psi_1}{\partial x_1} \\
e_{22}^0 - x_3\frac{\partial^2 u_3}{\partial x_2^2} + I_{2x_3}^{(k)}\frac{\partial\psi_2}{\partial x_2} \\
e_{12}^0 - 2x_3\frac{\partial^2 u_3}{\partial x_1\partial x_2} + I_{1x_3}^{(k)}\frac{\partial\psi_1}{\partial x_2} + I_{2x_3}^{(k)}\frac{\partial\psi_2}{\partial x_1}
\end{bmatrix}
\tag{7}
$$

where displacements in the x_1, x_2 and x_3 directions are indicated by $u_i(i=1,2,3)$, respectively, the strains containing nonlinear terms on the mid-surface are indicated by $e_{ij}^0(i,j=1,2)$, the functions associated with the transverse shear stresses in the lamina k^{th} of multilayer shell-type structural elements with double curvature consisting of CNT patterned layers are indicated by $I_{jx_3}^{(k)}(j=1,2)$, and are described as [39]:

$$
e_{11}^0 = \frac{\partial u_1}{\partial x_1} - \frac{u_3}{r_1} + \frac{1}{2}\left(\frac{\partial u_3}{\partial x_1}\right)^2, \quad e_{22}^0 = \frac{\partial u_2}{\partial x_2} - \frac{u_3}{r_2} + \frac{1}{2}\left(\frac{\partial u_3}{\partial x_2}\right)^2
$$
$$
e_{12}^0 = \frac{\partial u_2}{\partial x_1} + \frac{\partial u_1}{\partial x_2} + \frac{\partial u_3}{\partial x_1}\frac{\partial u_3}{\partial x_2}
\tag{8}
$$

and

$$
I_{1x_3}^{(k)} = \int_0^{x_3}\frac{1}{G_{13x_3}^{(k)}}\frac{df_{1x_3}^{(k)}}{dx_3}dx_3 \,, \, I_{2x_3}^{(k)} = \int_0^{x_3}\frac{1}{G_{23x_3}^{(k)}}\frac{df_{2x_3}^{(k)}}{dx_3}dx_3
\tag{9}
$$

Substituting relations (7) into (4) and after mathematical simplifications take the following form:

$$
\begin{bmatrix}
\sigma_{11}^{(k)} \\
\sigma_{22}^{(k)} \\
\sigma_{12}^{(k)}
\end{bmatrix}
=
\begin{bmatrix}
Q_{11\bar{x}_3}^{(k)} & Q_{12\bar{x}_3}^{(k)} & 0 \\
Q_{21\bar{x}_3}^{(k)} & Q_{22\bar{x}_3}^{(k)} & 0 \\
0 & 0 & Q_{66\bar{x}_3}^{(k)}
\end{bmatrix}
\begin{bmatrix}
e_{11}^0 - x_3\frac{\partial^2 u_3}{\partial x_1^2} \\
e_{22}^0 - x_3\frac{\partial^2 u_3}{\partial x_2^2} \\
e_{12}^0 - 2x_3\frac{\partial^2 u_3}{\partial x_1\partial x_2}
\end{bmatrix}
+
\begin{bmatrix}
I_{1x_3}^{(k)}Q_{11\bar{x}_3}^{(k)} & 0 & 0 \\
I_{1x_3}^{(k)}Q_{21\bar{x}_3}^{(k)} & 0 & 0 \\
0 & 0 & I_{1x_3}^{(k)}Q_{66\bar{x}_3}^{(k)}
\end{bmatrix}
\begin{bmatrix}
\frac{\partial\psi_1}{\partial x_1} \\
0 \\
\frac{\partial\psi_1}{\partial x_2}
\end{bmatrix}
$$
$$
+
\begin{bmatrix}
I_{2x_3}^{(k)}Q_{12\bar{x}_3}^{(k)} & 0 & 0 \\
I_{2x_3}^{(k)}Q_{22\bar{x}_3}^{(k)} & 0 & 0 \\
0 & 0 & I_{2x_3}^{(k)}Q_{66\bar{x}_3}^{(k)}
\end{bmatrix}
\begin{bmatrix}
\frac{\partial\psi_2}{\partial x_2} \\
0 \\
\frac{\partial\psi_2}{\partial x_1}
\end{bmatrix}
\tag{10}
$$

The force and moment components of multilayer shell-type structural elements with double curvature consisting of CNT patterned layers are found from the following integrals [1,35]:

$$
(T_{ij}, Q_j) = \sum_{k=1}^n \int_{-h/2+(k-1)h/N}^{-h/2+kh/N}\left(\sigma_{ij}^{(k)}, \sigma_{1j_1}^{(k)}\right)dx_3,
$$
$$
M_{ij} = \sum_{k=1}^n \int_{-h/2+(k-1)h/N}^{-h/2+kh/N}\sigma_{ij}^{(k)}x_3dx_3, \quad (i,j=1,2,j_1=2,3)
\tag{11}
$$

where the in-plane and shear forces are indicated by T_{ij} and Q_j, respectively, and moments are indicated by $M_{ij}(i,j=1,2)$.

The relationship of force components with the Airy stress function, Ψ is performed by the following equations [39]:

$$
(T_{11}, T_{22}, T_{12}) = h\left(\frac{\partial^2\Psi}{\partial x_2^2}, \frac{\partial^2\Psi}{\partial x_1^2}, -\frac{\partial^2\Psi}{\partial x_1\partial x_2}\right)
\tag{12}
$$

3.3. Governing equations

The governing equations of multilayer shell-type structural elements with double curvature consisting of CNT patterned layers are derived by using Hamilton principle as follows [1,5,38]:

$$
\frac{\partial M_{11}}{\partial x_1} + \frac{\partial M_{12}}{\partial x_2} - Q_1 + \rho_1 h^3\frac{\partial^3 u_3}{\partial x_1\partial\tau^2} - \rho_2 h^3\frac{\partial^2\psi_1}{\partial\tau^2} = 0
$$
$$
\frac{\partial M_{21}}{\partial x_1} + \frac{\partial M_{22}}{\partial x_2} - Q_2 + \rho_1 h^3\frac{\partial^3 u_3}{\partial x_2\partial\tau^2} - \rho_3 h^3\frac{\partial^2\psi_2}{\partial\tau^2} = 0
$$
$$
\frac{\partial Q_1}{\partial x_1} + \frac{\partial Q_2}{\partial x_2} + \frac{T_{11}}{r_1} + \frac{T_{22}}{r_2} + T_{11}\frac{\partial^2 u_3}{\partial x_1^2} + 2T_{12}\frac{\partial^2 u_3}{\partial x_1\partial x_2} + T_{22}\frac{\partial^2 u_3}{\partial x_2^2} - \bar{\rho}h\frac{\partial^2 u_3}{\partial\tau^2} = 0
\tag{13}
$$

$$
\frac{\partial^2 e_{11}^0}{\partial x_2^2} + \frac{\partial^2 e_{22}^0}{\partial x_1^2} - \frac{\partial^2 e_{12}^0}{\partial x_1\partial x_2} - \left(\frac{\partial^2 u_3}{\partial x_1\partial x_2}\right)^2 + \frac{\partial^2 u_3}{\partial x_1^2}\frac{\partial^2 u_3}{\partial x_2^2} + \frac{1}{r_2}\frac{\partial^2 u_3}{\partial x_1^2}
$$
$$
+ \frac{1}{r_1}\frac{\partial^2 u_3}{\partial x_2^2} = 0
\tag{14}
$$

where ρ_t and $\rho_i(i=1,2,3)$ are expressed as:

$$
\bar{\rho} = \sum_{k=1}^n \int_{-1/2+(k-1)/N}^{-1/2+k/N}\rho_t^{(k)}d\bar{x}_3, \quad \rho_1 = \sum_{k=1}^n \int_{-1/2+(k-1)/N}^{-1/2+k/N}\rho^{(k)}\bar{x}_3^2 d\bar{x}_3,
$$
$$
\rho_2 = \sum_{k=1}^n \int_{-1/2+(k-1)/N}^{-1/2+k/N}I_{1x_3}^{(k)}\rho^{(k)}\bar{x}_3 d\bar{x}_3, \quad \rho_3 = \sum_{k=1}^n \int_{-1/2+(k-1)/N}^{-1/2+k/N}I_{2x_3}^{(k)}\rho^{(k)}\bar{x}_3 d\bar{x}_3.
\tag{15}
$$

To express the basic equations with the Ψ, u_3, ψ_1, ψ_2, the relations (10) are substituted into integrals (11) and then resulting expressions with (12) are taken into account in the Eqs. (13) and (14), we obtain the nonlinear governing equations of multilayer shell-type structural elements with double curvature consisting of CNT patterned layers as:

$$L_{11}(\Psi) + L_{12}(u_3) + L_{13}(\psi_1) + L_{14}(\psi_2) = 0$$
$$L_{21}(\Psi) + L_{22}(u_3) + L_{23}(\psi_1) + L_{24}(\psi_2) = 0$$
$$L_{31}(\Psi) + L_{32}(u_3) + L_{33}(\psi_1) + L_{34}(\psi_2) + L_{35}(\Psi, u_3) = 0$$
$$L_{41}(\Psi) + L_{42}(u_3) + L_{43}(\psi_1) + L_{44}(\psi_2) + L_{45}(u_3, u_3) = 0$$

(16)

where

$$L_{11}(\Psi) = h\left[(S_{11} - S_{31})\frac{\partial^4}{\partial x_1^2 \partial x_2^2} + S_{12}\frac{\partial^4}{\partial x_1^4}\right],$$
$$L_{12}(u_3) = \rho_1 h^3 \frac{\partial^4}{\partial x_2^2 \partial \tau^2} - S_{13}\frac{\partial^4}{\partial x_2^4} - (S_{14} + S_{32})\frac{\partial^4}{\partial x_1^2 \partial x_2^2},$$
$$L_{13}(\psi_1) = S_{15}\frac{\partial^3}{\partial x_1^3} + S_{35}\frac{\partial^3}{\partial x_1 \partial x_2^2} - I_3\frac{\partial}{\partial x_1} - \rho_2 h^3 \frac{\partial^3}{\partial x_1 \partial \tau^2},$$
$$L_{14}(\psi_2) = (S_{18} + S_{38})\frac{\partial^3}{\partial x_1^2 \partial x_2}, \quad L_{21}(\Psi) = h\left[S_{21}\frac{\partial^4}{\partial x_2^4} + (S_{22} - S_{31})\frac{\partial^4}{\partial x_1^2 \partial x_2^2}\right],$$
$$L_{22}(u_3) = -(S_{32} + S_{23})\frac{\partial^4}{\partial x_1^2 \partial x_2^2} - S_{24}\frac{\partial^4}{\partial x_2^4} + \rho_1 h^3 \frac{\partial^4}{\partial x_2^2 \partial \tau^2},$$
$$L_{23}(\psi_1) = (S_{35} + S_{25})\frac{\partial^3}{\partial x_1 \partial x_2^2}, \quad L_{24}(\psi_2) = S_{38}\frac{\partial^3}{\partial x_2^2 \partial x_2} + S_{28}\frac{\partial^3}{\partial x_2^3} - I_4\frac{\partial}{\partial x_2} - \rho_3 h^3 \frac{\partial^3}{\partial x_2 \partial \tau^2},$$
$$L_{31}(\Psi) = h\left(\frac{1}{r_2}\frac{\partial^2}{\partial x_1^2} + \frac{1}{r_1}\frac{\partial^2}{\partial x_2^2}\right), L_{32}(u_3) = -\bar{\rho}h\frac{\partial^2}{\partial \tau^2}, \quad L_{33}(\varphi_1) = I_3\frac{\partial}{\partial x_1},$$
$$L_{34}(\varphi_2) = I_4\frac{\partial}{\partial x_2}, \quad L_{35}(\Psi, u_3) = h\left[\frac{\partial^2}{\partial x_2^2}\frac{\partial^2}{\partial x_1^2} - 2\frac{\partial^2}{\partial x_1 \partial x_2}\frac{\partial^2}{\partial x_1 \partial x_2} + \frac{\partial^2}{\partial x_1^2}\frac{\partial^2}{\partial x_2^2}\right],$$
$$L_{41}(\Psi) = h\left[B_{11}\frac{\partial^4}{\partial x_2^4} + (B_{12} + B_{21} + B_{31})\frac{\partial^4}{\partial x_1^2 \partial x_2^2} + B_{22}\frac{\partial^4}{\partial x_1^4}\right],$$
$$L_{42}(u_3) = -B_{23}\frac{\partial^4}{\partial x_1^4} - (B_{24} + B_{13} - B_{32})\frac{\partial^4}{\partial x_1^2 \partial x_2^2} - B_{14}\frac{\partial^4}{\partial x_2^4} + \left(\frac{1}{r_2}\frac{\partial^2}{\partial x_1^2} + \frac{1}{r_1}\frac{\partial^2}{\partial x_2^2}\right),$$
$$L_{43}(\psi_1) = B_{25}\frac{\partial^3}{\partial x_1^3} + (B_{15} + B_{35})\frac{\partial^3}{\partial x_1 \partial x_2^2}, \quad L_{44}(\psi_2) = (B_{28} + B_{38})\frac{\partial^3}{\partial x_1^2 \partial x_2} + B_{18}\frac{\partial^3}{\partial x_2^3},$$
$$L_{45}(u_3, u_3) = -\left(\frac{\partial^2}{\partial x_1 \partial x_2}\right)^2 + \frac{\partial^2}{\partial x_1^2}\frac{\partial^2}{\partial x_2^2},$$

(17)

where S_{ij}, B_{ij} and $I_k(k = 3, 4)$ are described in Appendix A.

4. Solution method

The functions u_3, ψ_1 and ψ_2 of multilayer shell-type structural elements with double curvature that the layers with CNT patterns are sought as follows [1,10]:

$$u_3 = u_{33}(\tau)\sin(\lambda_1 x_1)\sin(\lambda_2 x_2), \quad \psi_1 = \psi_{11}(\tau)\cos(\lambda_1 x_1)\sin(\lambda_2 x_2),$$
$$\psi_2 = \psi_{22}(\tau)\sin(\lambda_1 x_1)\cos(\lambda_2 x_2)$$

(18)

where $u_{33}(\tau)$, $\psi_{11}(\tau)$ and $\psi_{22}(\tau)$ are time dependent functions, $\lambda_1 = \frac{m\pi}{a_1}$ and $\lambda_2 = \frac{n\pi}{a_2}$, in which (m, n) is the vibration mode.

The deflection and angle functions of multilayer shell-type structural elements with double curvature consisting of CNT patterned layers in the form of (18), mathematically satisfies the following simply supported boundary conditions:

$$u_3 = 0, \quad M_{11} = 0, \quad \psi_2 = 0, \quad \text{as } x_1 = 0 \text{ and } x_1 = a_1$$
$$u_3 = 0, \quad M_{22} = 0, \quad \psi_1 = 0, \quad \text{as } x_2 = 0 \text{ and } x_2 = a_2$$

(19)

To find the Airy stress function (Ψ) depending on the function $u_{33}(\tau)$ from particular solution of the fourth inhomogeneous differential equation of system (16), the expression (18) is substituted into the fourth equation of system (16), and it takes the following form:

$$\alpha_1\frac{\partial^4\Psi}{\partial x_2^4} + \alpha_2\frac{\partial^4\Psi}{\partial x_1^2 \partial x_2^2} + \alpha_3\frac{\partial^4\Psi}{\partial x_1^4} = 0.5\alpha_{14}u_{33}^2(\tau)[\cos(2\lambda_1 x_1) + \cos(2\lambda_2 x_2)]$$
$$+ \alpha_{11}u_{33}(\tau)\sin(\lambda_1 x_1)\sin(\lambda_2 x_2)$$

(20)

The symbols used here are defined as follows:

$$\alpha_1 = B_{11}h; \quad \alpha_2 = (B_{12} + B_{21} + B_{31})h; \quad \alpha_3 = B_{22}h,$$
$$\alpha_{11} = B_{23}\lambda_1^4 + (B_{24} + B_{13} - B_{32})\lambda_1^2\lambda_2^2 + B_{14}\lambda_2^4 + \frac{\lambda_1^2}{r_2} + \frac{\lambda_2^2}{r_1}, \quad \alpha_{14} = \lambda_1^2\lambda_2^2.$$

(21)

The particular solution of the inhomogeneous differential equation (20) is sought according to the shape of the right-hand side as follows:

$$\Psi = A\cos(2\lambda_1 x_1) + B\cos(2\lambda_2 x_2) + C\sin(\lambda_1 x_1)\sin(\lambda_2 x_2)$$

(22)

where A, B and C are unknown coefficients.

Substituting the expression (22) on the left-hand side of Eq. (20), it becomes:

$$\alpha_1\frac{\partial^4\Psi}{\partial x_2^4} + \alpha_2\frac{\partial^4\Psi}{\partial x_1^2 \partial x_2^2} + \alpha_3\frac{\partial^4\Psi}{\partial x_1^4} = 16A\lambda_1^4\alpha_3\cos(2\lambda_1 x_1) + 16\lambda_2^4 B\alpha_1\cos(2\lambda_2 x_2)$$
$$+ C(\alpha_1\lambda_2^4 + \alpha_2\lambda_1^2\lambda_2^2 + \alpha_3\lambda_1^4)$$

(23)

From the equality of the left sides of (20) and (23), the coefficients A, B and C are found as follows:

$$A = \frac{\alpha_{14}u_{33}^2(\tau)}{32\lambda_1^4\alpha_3}, \quad B = \frac{\alpha_{14}u_{33}^2(\tau)}{32\lambda_2^4\alpha_1}, \quad C = \frac{\alpha_{11}u_{33}(\tau)}{\alpha_1\lambda_2^4 + \alpha_2\lambda_2^2\lambda_1^2 + \alpha_3\lambda_1^4}$$

(24)

Substituting (23) into (21) and then by taking (24), the following expression for the Airy stress function is obtained:

$$\Psi = \beta_1 u_{33}^2(\tau)\cos(2\lambda_1 x_1) + \beta_2 u_{33}^2(\tau)\cos(2\lambda_2 x_2)$$
$$+ \beta_3 u_{33}(\tau)\sin(\lambda_1 x_1)\sin(\lambda_2 x_2)$$

(25)

where

$$\beta_1 = \frac{1}{32B_{22}h}\left(\frac{\lambda_2}{\lambda_1}\right)^2, \quad \beta_2 = \frac{1}{32B_{11}h}\left(\frac{\lambda_1}{\lambda_2}\right)^2,$$
$$\beta_3 = \frac{B_{23}\lambda_1^4 + (B_{24} + B_{13} - B_{32})\lambda_1^2\lambda_2^2 + B_{14}\lambda_2^4 + \frac{\lambda_1^2}{r_2} + \frac{\lambda_2^2}{r_1}}{h\left[B_{11}\lambda_2^4 + (B_{12} + B_{21} + B_{31})\lambda_1^2\lambda_2^2 + B_{22}\lambda_1^4\right]}$$

(26)

By using Galerkin method to first three equations of set (16) in intervals of $0 \leqslant x_1 \leqslant a_1$ and $0 \leqslant x_2 \leqslant a_2$, we obtain,

$$\mu_{11}u_{33} + \mu_{11}^{NL}u_{33}^2 + \mu_{11}^\tau\frac{d^2u_{33}}{d\tau^2} + \mu_{12}\psi_{11} + \mu_{12}^\tau\frac{d^2\psi_{11}}{d\tau^2} + \mu_{13}\psi_{22} = 0,$$
$$\mu_{21}u_{33} + \mu_{21}^{NL}u_{33}^2 + \mu_{21}^\tau\frac{d^2u_{33}}{d\tau^2} + \mu_{22}\psi_{11} + \mu_{23}\psi_{22} + \mu_{23}^\tau\frac{d^2\psi_{22}}{d\tau^2} = 0,$$
$$\bar{\rho}h\frac{d^2u_{33}}{d\tau^2} + \mu_{31}u_{33} + \mu_{31}^{NL}u_{33}^2 + \mu_{32}u_{33}^3 + \mu_{33}\psi_{11} + \mu_{34}\psi_{22} = 0$$

(27)

where $\mu_{ij}(i = 1, 2, 3, j = 1, 2, 3, 4)$ are parameters that characterize the properties of multilayer shell-type structural elements with double curvature consisting of CNT patterned layers and are given in Appendix B.

By ignoring from set of Eq. (27), because of the smallness of the inertia terms with the top index τ and eliminating the functions ψ_{11} and ψ_{22} from the obtained equations, Considering this matter (i.e., $\mu_{11}^\tau = \mu_{12}^\tau = \mu_{21}^\tau = \mu_{23}^\tau = 0$) in Eq. (27), and excluding ψ_{11} and ψ_{22} from Eq. (27), one gets

$$\frac{d^2w}{d\tau^2} + (\omega_{Lin}^{SDT})^2 w + K_{11}^{sdt}w^2 + K_{12}^{sdt}w^3 = 0$$

(28)

where $w = u_{33}/h$ and ω_{Lin}^{sdt} is the linear frequency (LF) of multilayer shell-type structural elements with double curvature consisting of CNT patterned layers within SDT and defined as:

$$\omega_{Lin}^{sdt} = \sqrt{\frac{\mu_{31} + \mu_{33}\frac{\mu_{11}\mu_{23} - \mu_{21}\mu_{13}}{\mu_{22}\mu_{13} - \mu_{12}\mu_{23}} - \mu_{34}\left(\frac{\mu_{21}}{\mu_{23}} + \frac{\mu_{22}}{\mu_{23}}\frac{\mu_{11}\mu_{23} - \mu_{21}\mu_{13}}{\mu_{22}\mu_{13} - \mu_{23}\mu_{12}}\right)}{\rho^- h}}$$

(29)

and

$$K_{11}^{sdt} = \frac{\bar{\mu}_{31}^{NL}}{\rho h}, \quad K_{12}^{sdt} = \frac{\mu_{32}}{\rho h^2}$$

$$\bar{\mu}_{31} = \mu_{31} + \mu_{33}\frac{\mu_{11}\mu_{23} - \mu_{21}\mu_{13}}{\mu_{22}\mu_{13} - \mu_{12}\mu_{23}} - \mu_{34}\left(\frac{\mu_{21}}{\mu_{23}} + \frac{\mu_{22}}{\mu_{23}}\frac{\mu_{11}\mu_{23} - \mu_{21}\mu_{13}}{\mu_{22}\mu_{13} - \mu_{23}\mu_{12}}\right)$$

$$\bar{\mu}_{31}^{NL} = \mu_{31}^{NL} - \frac{\mu_{33}\left(\mu_{11}^{NL}\mu_{23} - \mu_{13}\mu_{21}^{NL}\right)}{\mu_{12}\mu_{23} - \mu_{13}\mu_{22}} - \frac{\mu_{34}\mu_{21}^{NL}}{\mu_{23}} + \frac{\mu_{34}\mu_{22}}{\mu_{23}}\frac{\mu_{11}^{NL}\mu_{23} - \mu_{13}\mu_{21}^{NL}}{\mu_{12}\mu_{23} - \mu_{13}\mu_{22}}$$

(30)

By applying the variation principle to Eq. (28) and using the semi-inverse method, let's construct the following integral [39–41]:

$$\Gamma(w) = \int_0^{T/4}\left\{-\frac{1}{2}\left[\frac{dw^2(\tau)}{d\tau}\right]^2 + (\omega_{Lin}^{sdt})^2\left[\frac{w^2(\tau)}{2} + K_{11}^{sdt}\frac{w^3(\tau)}{3(\omega_{Lin}^{sdt})^2} + K_{11}^{sdt}\frac{w^4(\tau)}{4(\omega_{Lin}^{sdt})^2}\right]\right\}d\tau$$

(31)

where, the symbol $T = 2\pi/\omega_{NL}^{sdt}$ indicates the large amplitude vibration period and ω_{NL}^{sdt} indicates the nonlinear vibration frequency of multilayer shell-type structural elements with double curvature consisting of CNT patterned layers.

The initial conditions for the movement of multilayer shell-type structural elements with double curvature consisting of CNT patterned layers are mathematically defined as follows [40,41]:

$$w(\tau)|\tau = 0 = w_0 \text{ and } \frac{dw(\tau)}{d\tau}|\tau = 0 = 0 \tag{32}$$

To satisfy the initial conditions (36), in the first approximation, $w(t)$ is expressed as:

$$w(\tau) = \bar{w}\cos(\omega_{NL}^{sdt}\tau) \tag{33}$$

where $\bar{w} = w_{max}$ is the maximum amplitude of the deflection w. When the expression (33) is substituted into the Eq. (31) and the transformation $t = \omega_{NL}^{sdt}\tau$ is made, it turns into the following form after integration [39–41]:

$$\Gamma(\bar{w}, \omega_{NL}^{sdt}) = -\frac{\pi\bar{w}^2\omega_{NL}^{sdt}}{8} + \frac{(\omega_{Lin}^{sdt})^2}{\omega_{NL}^{sdt}}\left[\frac{\pi\bar{w}^2}{8} + \frac{2k_{12}\bar{w}^3}{9(\omega_{Lin}^{sdt})^2} + \frac{3k_{13}\pi\bar{w}^4}{64(\omega_{Lin}^{sdt})^2}\right] \tag{34}$$

When the function (34) is examined, can be seen that $\frac{\partial\Gamma(\bar{w},\omega_{NL}^{sdt})}{\partial\omega_{Nl}^{sdt}} < 0$, therefore, from the condition $\frac{\partial\Gamma(\bar{w},\omega_{NL}^{sdt})}{\partial\bar{w}} = 0$, the $\bar{w}$ dependence of nonlinear frequency for multilayer shell-type structural elements with double curvature consisting of CNT patterned layers becomes as follows:

$$\omega_{NL}^{sdt} = \left[(\omega_{Lin}^{sdt})^2 + \frac{8}{3\pi}K_{11}^{sdt}\bar{w} + \frac{3}{4}K_{12}^{sdt}\bar{w}^2\right]^{1/2} \tag{35}$$

The $\bar{w}$ dependence of nondimensionalized non-linear frequency of multilayer shell-type structural elements with double curvature consisting of CNT patterned layers is expressed as:

$$\omega_{1NL}^{sdt} = \omega_{NL}^{sdt}h\sqrt{\frac{\rho_m^{(k)}}{E_m^{(k)}}} \tag{36}$$

The $\bar{w}$ dependence of the ratio of non-linear frequency to linear frequency for multilayer shell-type structural elements with double curvature consisting of CNT patterned layers is obtained as follows:

$$\left(\frac{\omega_{NL}^{sdt}}{\omega_{Lin}^{sdt}}\right)^2 = 1 + \frac{8}{3\pi}\frac{K_{11}^{sdt}\bar{w}}{(\omega_{Lin}^{sdt})^2} + \frac{3}{4}\frac{K_{12}^{sdt}\bar{w}^2}{(\omega_{Lin}^{sdt})^2} \tag{37}$$

If we neglect the influence of shear deformations, the obtained formulas for linear and nonlinear frequencies for multilayer shell-type structural elements with double curvature consisting of CNT patterned layers turn into formulas within the classical shell theory (CST) framework.

The expressions (29), (35)–(37) for multilayer shell-type structural elements with double curvature also apply to multilayer spherical shells as $r_1 = r_2$, multilayer hypar shells as $r_1 = -r_2$, multilayer cylindrical panels as $r_1 \to \infty$ and multilayer plates as $r_1 = r_2 \to \infty$.

5. Discussion

In this section, after confirming the accuracy of obtained results by comparisons, the effect of changing the r_1/a_1 and a_1/a_2 ratios, number and arrangement of layers on the dependence $\bar{w}$ of the nonlinear free vibration frequency for multilayer shell-type structural elements with double curvature consisting of CNT patterned layers are presented. The shear stresses of multilayer shell-type structural elements with double curvature consisting of CNT patterned layers are used as, $f_j^{(k)}(x_3) = x_3(1 - 4x_3^2/3h^2)$, $(j = 1,2)$ [1]. Arrangement and number

of layers of multilayer shell-type structural elements made of patterned CNT layers are plotted in Fig. 3.

The Young's modulus, Poisson ratio and density of the lamina k^{th} made of polymethyl methacrylate (PMMA) are as follows: $E_m^{(k)} = 2.5$ GPa, $\nu_m^{(k)} = 0.34$ and $\rho_m^{(k)} = 1150$ kg/m³. The material properties of single-walled CNTs in the lamina k^{th} are defined as: $E_{11cn}^{(k)} = 5.6466$ TPa, $E_{22cn}^{(k)} = 7.08$ TPa, $G_{12cn}^{(k)} = 1.9445$ TPa, $\nu_{12cn}^{(k)} = 0.175$ and $\rho_{cn}^{(k)} = 1400$ kg/m³. The efficiency parameters and total volume fraction (VF) of CNTs in the lamina k^{th} are given in Table 1 [20].

5.1. Comparisons

The purpose of this subsection is to show the accuracy of the results obtained in accordance with the results reported in the literature. Alijani et al. [31] and Bich et al. [32] performed numerical calculations within the scope of FSDT for the nondimensional linear frequency parameters of homogeneous isotropic monolayer shell-type structural elements using different solution methods (see, Table 2). In these studies, values of linear vibration frequencies of monolayer spherical and hypar shells, and plate for $E_{11}^{(1)} = E_{22}^{(1)} = E_m^{(1)} = 70$ GPa, $\nu_{12}^{(1)} = \nu_m^{(1)} = 0.3177$, $\rho_m^{(1)} = 2702$ kg/m³, $a_1/a_2 = 1$, $a_1 = 10h$ and $V_{cn}^{*(1)} = 0$ data are included. The expression (29) is used for the calculation of linear frequency values in our study. Using these data and taking into account $k = 1$ in expression (29), a comparison is made with the results of these studies. It can be seen from Table 2 that the results are in agreement with the results of refs. [31,32].

In the second example, the nondimensional frequency parameter $\Omega_{1L} = \Omega_L(a_1^2/h)\sqrt{\rho_m^{(1)}/E_m^{(1)}}$ values of different CNT patterned monolayer spherical and hypar shells, cylindrical panels and plates are compared with the study of Pouresmaeeli and Fazelzadeh [21] for $(m, n) = (1,1)$, $a_1/h = 20$, $a_1/a_2 = 1$ and presented in Table 3. The expression (29) is used for the calculation of linear frequency values. Young's modulus, Poisson ratio and density of the lamina k^{th} made of PMMA are as follows: $E_m^{(1)} = 2.1$ GPa, $\nu_m^{(1)} = 0.34$ and $\rho_m^{(1)} = 1150$ kg/m³. In addition, the mechanical properties of CNT, is defined as follows: $E_{11cn}^{(1)} = 5.6466$ TPa, $E_{22cn}^{(1)} = 7.08$ TPa, $G_{12cn}^{(1)} = 1.9445$ TPa, $\nu_{12cn}^{(1)} = 0.175$ and $\rho_{cn}^{(1)} = 1400$ kg/m³. The CNT efficiency parameters in the monolayer shells are used in ref. [21] as: $\eta_1^{(1)} = 0.149$, $\eta_2^{(1)} = \eta_3^{(1)} = 0.934$ for $V_{cn}^{*(1)} = 0.11$, $\eta_1^{(1)} = 0.15$, $\eta_2^{(1)} = \eta_3^{(1)} = 0.941$ for $V_{cn}^{*(1)} = 0.14$ and $\eta_1^{(1)} = 0.149$, $\eta_2^{(1)} = \eta_3^{(1)} = 1.381$ for $V_{cn}^{*(1)} = 0.17$. As can be seen from Table 3, the results are in good agreement.

5.2. Specific analysis

In this subsection, the influences of number and arrangement of layers, CNT patterns and volume fractions on the nondimensional non-linear frequencies of multilayer spherical and hypar shell consisting of CNT patterned layers are investigated in detail for different sizes depending on the dimensionless amplitude parameter, $\bar{w}$. Fig. 4 presents the multilayer hypar shell consisting of CNT patterned layers.

$\bar{w}$ dependence of the nondimensional nonlinear frequency (NDNLF) values of multilayer spherical (ML-SSs) and hypar (ML-HSs) shells consisting of U and X type CNT patterned layers for $a_1/a_2 = 1, 1.5, 2$, $r_1/a_1 = 2$, $a_1/h = 15$; $(m,n) = (1,1)$ and $V_{cn}^{*(k)} = 0.28$ are given in Table 4. As seen from Table 4, six different consecutive layer arrangements,$(0°)$, $(90°)$, $(0°/90°/0°)$, $(90°/0°/90°)$, $(0°/90°/90°/0°)$ and $(90°/0°/0°/90°)$, are considered with U and X patterns. As a_1/a_2 increases, NDNLF values increase in both shells, for both SDT and CST cases and as $\bar{w}$ increases, they increase when $\bar{w} > 0.5$, while decreasing when $\bar{w} \leq 0.5$. When the two shells are compared with each other, both for SDT and CST cases, NDNLF values obtained for ML-SSs
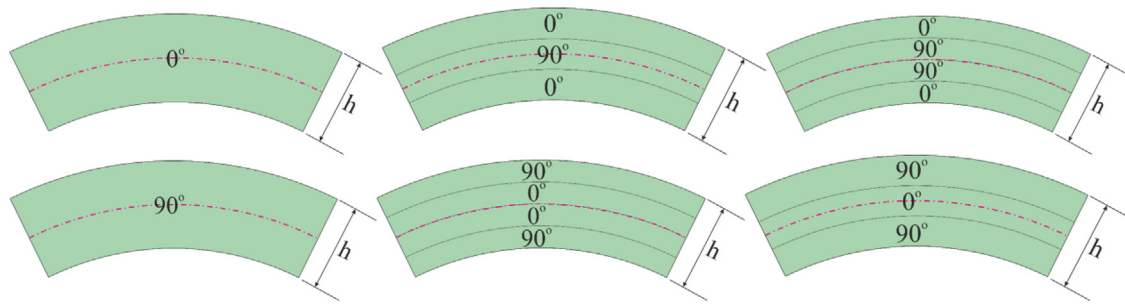
Fig. 3. Arrangement and number of layers of multilayer shallow shells with double curvature, made of patterned CNT layers.

Table 1
Efficiency parameters and total VF of CNTs in the lamina k^{th}.

$V_{cn}^{*(k)}$	$\eta_1^{(k)}$	$\eta_2^{(k)}$	$\eta_3^{(k)}$
1.2×10^{-1}	1.37×10^{-1}	1.022	7.15×10^{-1}
1.7×10^{-1}	1.42×10^{-1}	1.626	1.138
2.8×10^{-1}	1.41×10^{-1}	1.585	1.109

being larger for each of $a_1/a_2 = 1$ and $\bar{w} < 1.5$, $a_1/a_2 = 1.5$ and $\bar{w} < 1.25$, $a_1/a_2 = 2$ and $\bar{w} < 1$, cases, for cases other than those, they are larger for ML-HSs. When $(0°/90°/0°)$ and $(0°/90°/90°/0°)$ layer order is compared with $(0°)$, for both shells, NDNLF values for CST case in three and four layered shells being larger, for SDT case, while they are larger in the range $0.25 \leqslant \bar{w} \leqslant 0.75$ for three layered shells they are smaller for all $\bar{w}$ in the four layered ones. When $(90°/0°/90°)$ and $(90°/0°/0°/90°)$ layer order is compared with $(90°)$ for both shells, in the CST case, NDNLF values are smaller for the three layered shells, while they are larger for the four layered ones, whereas, in the SDT case, they are larger for the three layered shells in the range $0.25 \leqslant \bar{w} \leqslant 0.75$ and smaller in the four layered ones for all $\bar{w}$ values. Furthermore, even only a change of the angle of direction causes an increase in the NDNLF values, meaning that, in all cases NDNLF values in layered shells with $(90°)$ outer layers are larger than the values in the ones with $(0°)$ outer layers. Besides, while the NDNLF values for the shells with $(0°)$ outer layers are smaller for the four layered ones than those for the three-layered ones, in the case of the shells with $(90°)$ outer layers, they are larger for the shells with four layers than those with three.

In both shells, the effect of shear deformation (SD) on the NDNLF values decrease with increasing a_1/a_2 ratios and when $\bar{w} \leqslant 0.5$ they increase, whereas, when $\bar{w} > 0.5$ they decrease. Additionally, SD effect is greater for the X pattern. For example, with $(0°/90°/0°)$ layer order and $a_1/a_2 = 1$ in the U pattern for ML-SSs and ML-HSs, respectively, while increasing from (19.66%) to (23.49%) and from (22.59%) to (25.94%) when $\bar{w} \leqslant 0.5$, decreases from (23.49%) to (14.31%) and from (25.97%) to (14.07%) when $\bar{w} > 0.5$. Likewise, in the X pattern, for both shells in the same order, the foregoing ranges, when $\bar{w} \leqslant 0.5$ are from (22.13%) to (24.97%) and from (24.53%) to (26.78%) and when $\bar{w} > 0.5$ from (24.97%) to (17.76%) and from (26.78%) to

(17.52%), respectively. Again with $(0°/90°/0°)$ layer order but when $\bar{w} = 0$ or a linear frequency, as a_1/a_2 passes from 1 to 2 for both shells, in the foregoing sequence, decreases, respectively, in the U pattern from (19.66%) to (17.67%) and from (22.59%) to (19.96%) and in the X pattern from (22.13%) to (20.78%) and from (24.53%) to (22.91%).

When the two shells are compared with each other, for the cases, $a_1/a_2 = 1$ and $\bar{w} < 1.5$, $a/b = 1.5$ and $\bar{w} < 1.25$, $a_1/a_2 = 2$ and $\bar{w} < 1$, the SD effect is greater for ML-HSs, but for all other cases it is greater for ML-SSs. Considering both shells, the greatest SD effect difference (2.94%) is obtained for $(0°/90°/90°/0°)$ layer order. When $(0°/90°/0°)$ and $(0°/90°/90°/0°)$ layer orders are compared with $(0°)$, when $\bar{w} \leqslant 1$ the SD effect is greater in the three- and four-layer cases in both shells. On the other hand, when $(90°/0°/90°)$ and $(90°/0°/0°/90°)$ layer orders are compared with $(90°)$, when $\bar{w} \leqslant 1$ the SD effect is less in the three- and four-layer cases in both shells. For example, for $a_1/a_2 = 1$ in the X pattern, the maximum SD effects for ML-SSs and ML-HSs, respectively, in $(0°)$ (24.84%) and (26.61%), in $(90°)$ (29.19%) and (30.96%), in $(0°/90°/0°)$ (24.97%) and (26.78%), in $(90°/0°/90°)$ (29.04%) and (30.80%), in $(0°/90°/90°/0°)$ (25.38%) and (27.21%) and in $(90°/0°/0°/90°)$ (28.68%) and (30.42%). As a_1/a_2 increases, the X pattern effect on the NL-FVF values, increase when $\bar{w} \leqslant 0.5$ and decrease when $\bar{w} > 0.5$ in both shells. This increase or decrease are more important in ML-HSs for SDT when $\bar{w} > 0.5$ and $a_1/a_2 < 1.5$. On the other hand, this effect takes greater values for CST. For example, in the $(0°/90°/90°/0°)$ layer order for SDT when $a_1/a_2 = 1$ in ML-SSs and ML-HSs, respectively, it increases from (15.22%) to (19.71%) and from (17.73%) to (22.24%) when $\bar{w} > 0.5$, while decreasing from (19.71%) to (8.75 %) and from (22.24%) to (8.64%) when $\bar{w} > 0.5$. Likewise, in the $(0°/90°/90°/0°)$ layer order for CST when $a_1/a_2 = 1$, in ML-SSs and ML-HSs , respectively, increases from (18.78%) to (21.91%) and from (20.67%) to (23.44%) for $\bar{w} \leqslant 0.5$, while decreasing from (21.91%) to (13.29%) and from (23.44%) to (13.15%) when $\bar{w} > 0.5$. For $(0°/90°/90°/0°)$ layer order, this time, keeping $\bar{w} = 0.5$ fixed, as a_1/a_2 passes from 1 to 2 in ML-SSs and ML-HSs, respectively, decreases from (19.71%) to (15.90%) and from (22.24%) to (16.67%) for SDT, while from (21.91%) to (18.30%) and from (23.44%) to (28.90%) for CST.

Table 2
Comparison of nondimensional linear frequency parameter of structural elements.

Structural elements	a_1/r_1	a_2/r_2	$\bar{\Omega}_L = \Omega_L h \sqrt{\rho_m^{(1)}/E_m^{(1)}}$		
			Ref. [31]	Ref. [32]	Present study
Spherical shell	0.5	0.5	7.79×10^{-2}	7.67×10^{-2}	7.69×10^{-2}
Hypar shell	0.5	-0.5	5.97×10^{-2}	5.92×10^{-2}	5.84×10^{-2}
Plate	0	0	5.97×10^{-2}	5.81×10^{-2}	5.84×10^{-2}

Table 3

Comparison the dimensionless linear frequency parameter of CNT patterned monolayer spherical and hypar shells, cylindrical panels and plates.

| a_1/r_1	a_2/r_2	$V_{cn}^{*(1)}$	$\Omega_{1L} = \Omega_L(a_1^2/h)\sqrt{\rho_m^{(1)}/E_m^{(1)}}$					
			U		V		X	
			Ref. [21]	Present study	Ref. [21]	Present study	Ref. [21]	Present study
0.5	0.5	0.11	20.238	20.286	18.543	18.685	22.432	22.493
		0.14	21.655	21.756	19.779	19.966	23.997	24.064
		0.17	25.021	25.158	22.951	23.165	27.883	27.893
0.5	−0.5	0.11	17.106	17.332	14.809	15.114	19.588	19.853
		0.14	18.626	18.924	16.181	16.544	21.225	21.512
		0.17	21.093	21.423	18.225	18.645	24.274	24.524
0.5	0	0.11	18.126	18.116	16.060	16.150	20.548	20.545
		0.14	19.628	19.670	17.391	17.524	22.179	22.178
		0.17	22.380	22.415	19.799	19.949	25.488	25.408
0	0	0.11	18.008	17.332	15.701	15.113	20.624	19.853
		0.14	19.608	18.924	17.147	16.544	22.349	21.512
		0.17	22.207	21.424	19.315	18.645	25.557	24.524
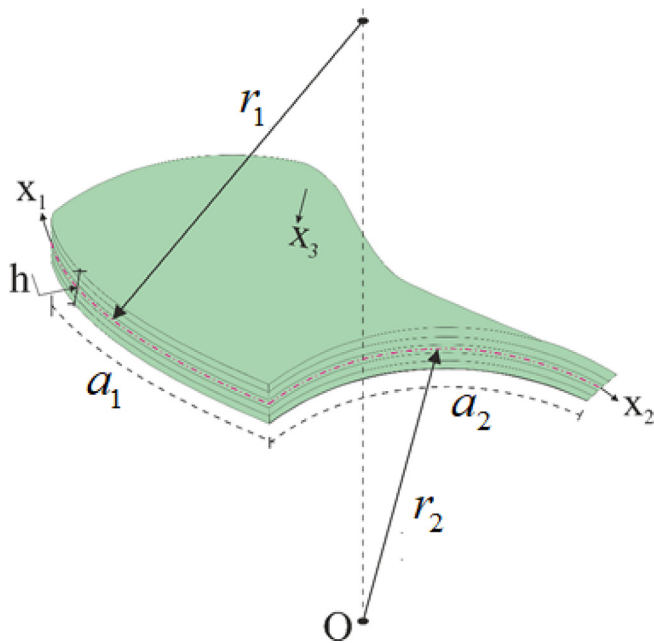
Fig. 4. Multilayer hypar shell consisting of CNT patterned layers.

The variation of NDNLF values of ML-SSs and ML-HSs consisting of O type CNT patterned layers with $\bar{w}$ for $a_1/a_2 = 0.5$, $r_1/a_1 = 2$, $a_1/h = 15$, $(m,n) = (1,1)$ and $V_{CN}^* = 0.12$ are given in Fig. 5. As seen from Fig. 5a and b six different layer orders $(0°)$, $(90°)$, $(0°/90°/0°)$, $(90°/0°/90°)$, $(0°/90°/90°/0°)$ and $(90°/0°/0°/90°)$ are considered with O pattern. In both shells for both SDT and CST, as $\bar{w}$ increases, while NDNLF values decrease when $\bar{w} \leqslant 0.5$, they increase when $\bar{w} > 0.5$. When the two shells are compared with each other, for both SDT and CST the NDNLF values for ML-SSs are greater and in both shells the greatest NDNLF value is obtained for $(90°)$ monolayer shell at $\bar{w} = 1.5$, while the least for $(0°)$ monolayer shell at $\bar{w} = 0.5$. It is observed that in both shells and for both SDT and CST, the NDNLF values for three and four layered shells are greater, when $(0°/90°/0°)$ and $(0°/90°/90°/0°)$ layer orders are compared with $(0°)$ monolayer shell, and smaller when $(90°/0°/90°)$ and $(90°/0°/0°/90°)$ are compared with $(90°)$. As $\bar{w}$ varies the SD effect on the NDNLF values increase for $\bar{w} \leqslant 0.5$, but decrease for $\bar{w} > 0.5$. When the two shells are compared with each other, the SD effect is about (%2) less for ML-SSs. In both shells, when

$(0°/90°/0°)$ and $(0°/90°/90°/0°)$ layer orders are compared with $(0°)$ monolayer shell, and $(90°/0°/90°)$ and $(90°/0°/0°/90°)$ layered shells are compared with $(90°)$ monolayer shell, respectively, in the former case in three layered shells about (0.7%) and in four layered shells about (1.2%) greater SD effect, whereas, in the latter in three layered shells about (0.7%) and in the four layered shells about (1.2%) less SD effect is observed. The SD effect is greater for layered shells having 90° outer layers than those having $(0°)$ outer layers. In this context, in both shells, the maximum SD effect differences between $(90°)$ and $(0°)$; $(90°/0°/90°)$ and $(0°/90°/0°)$; $(90°/0°/0°/90°)$ and $(0°/90°/90°/0°)$ are, respectively, $(\%3.3)$, (1.9%) and (0.9%) .

The variation of the NDNLF values of ML-SSs and ML-HSs with $\bar{w}$ for $r_1/a_1 = 2, 2.5, 3$, $a_1/a_2 = 1$, $a_1/h = 15$, $(m,n) = (1,1)$ and $V_{cn}^{*(k)} = 0.17$ are given in Fig. 6. As seen from Fig. 6a–d two different layer orders, $(90°)$ and $(90°/0°/0°/90°)$, are considered with U and V patterns. In both shells depending on the increase in $\bar{w}$ and the three values of r_1/a_1 the variation of NDNLF values have different features. In ML-HSs for both layer orders, they decrease in the range $\bar{w} \leqslant 0.5$ and increase in the range $\bar{w} > 0.5$ when $r_1/a_1 < 2.5$ and decrease in the range $\bar{w} \leqslant 0.25$ and increase in the range $\bar{w} > 0.25$ when $r_1/a_1 \geqslant 2.5$. In ML-SSs, for both layer orders, they decrease in the range $\bar{w} \leqslant 0.5$ and increase in the range $\bar{w} > 0.5$ when $r_1/a_1 < 3$ and decrease in the range $\bar{w} \leqslant 0.25$ and increase in the range $\bar{w} > 0.25$ when $r_1/a_1 = 3$. In ML-HSs the NDNLF values increase with the increase of r_1/a_1 and in ML-SSs with the increase of r_1/a_1, decrease in the range $\bar{w} < 0.5$ and increase in the range $\bar{w} \geqslant 0.5$. The foregoing increase and decrease are faster for high values of $\bar{w}$. When the two shells are compared with each other, for both SDT and CST, in the ranges $r_1/a_1 = 2$ at $0 \leqslant \bar{w} \leqslant 1.25$, $r_1/a_1 = 2.5$ at $\bar{w} > 1$, and $r_1/a_1 = 3$ at $\bar{w} \geqslant 1$, while the NDNLF values for ML-SSs being greater, the difference between the values for them decreases as $\bar{w}$ or r_1/a_1 increase. If the layer orders are compared with each other, in both shells NL-FVF values found for $(90°/0°/0°/90°)$ are smaller.

In both shells, as $\bar{w}$ increases the SD effect on the NDNLF values starts increasing about $(\%2)$ and later decreases about (3.5%) and the increase and decrease are more pronounced for $r_1/a_1 = 3$ and $(90°)$ in the U pattern. When $\bar{w} = 0.5$ in the U pattern as r_1/a_1 increases from 2 to 2.5, SD effect in ML-SSs and ML-HSs with V pattern, respectively, decreases $(\%0.11)$ and (1.69%) in the $(90°)$ layer order and (0.05%) and (1.14%) in the $(90°/0°/0°/90°)$ layer order, whereas, as r_1/a_1 increases from 2.5 to 3, increases (4.84%) and (4.65%) in the $(90°)$ layer order and (4.63%) and (4.44%) in the $(90°/0°/0°/90°)$ layer order. The SD effect difference between the two shells being highest (3.03%) for $(90°)$ and $(\%2.9)$ for

Table 4
$\bar{w}$ dependence of NDNLF for (a) ML-SS and (b) ML-HS consisting of U and X type CNT patterned layers with different arrangements and a_1/a_2 ratio.

a/b	$\bar{w}$	Multilayer spherical shells ($V_{cn}^{*(k)} = 0.28$)											
		0°				90°				0°/90°/0°			
		U		X		U		X		U		X	
		SDT	CST	SDT	CST	SDT	CST	SDT	CST	SDT	CST	SDT	CST
1	0	1.031	1.281	1.193	1.530	1.082	1.408	1.252	1.690	1.033	1.285	1.193	1.532
	0.5	0.915	1.189	1.093	1.453	0.950	1.310	1.139	1.608	0.910	1.189	1.091	1.454
	1	1.002	1.257	1.165	1.509	1.060	1.392	1.231	1.674	1.006	1.264	1.166	1.511
	1.5	1.249	1.462	1.383	1.682	1.354	1.626	1.490	1.873	1.272	1.485	1.390	1.690
1.5	0	1.137	1.380	1.303	1.631	1.182	1.499	1.356	1.782	1.139	1.384	1.303	1.633
	0.5	1.014	1.280	1.195	1.546	1.045	1.393	1.236	1.692	1.009	1.280	1.193	1.546
	1	1.092	1.343	1.261	1.597	1.145	1.470	1.321	1.755	1.096	1.349	1.262	1.600
	1.5	1.337	1.548	1.478	1.774	1.434	1.705	1.578	1.956	1.358	1.570	1.484	1.781
2	0	1.335	1.568	1.515	1.828	1.372	1.675	1.560	1.965	1.336	1.572	1.515	1.830
	0.5	1.221	1.472	1.413	1.744	1.245	1.572	1.446	1.876	1.217	1.472	1.411	1.745
	1	1.316	1.552	1.496	1.813	1.358	1.663	1.546	1.954	1.319	1.557	1.497	1.815
	1.5	1.582	1.783	1.739	2.017	1.664	1.921	1.823	2.180	1.600	1.802	1.744	2.023
		90°/0°/90°				0°/90°/90°/0°				90°/0°/0°/90°			
1	0	1.080	1.404	1.252	1.688	1.037	1.297	1.195	1.541	1.077	1.393	1.251	1.681
	0.5	0.956	1.310	1.141	1.608	0.911	1.198	1.090	1.461	0.956	1.301	1.142	1.601
	1	1.057	1.385	1.230	1.672	1.011	1.277	1.168	1.520	1.052	1.374	1.228	1.664
	1.5	1.332	1.605	1.484	1.867	1.287	1.504	1.399	1.704	1.319	1.587	1.475	1.854
1.5	0	1.181	1.495	1.356	1.780	1.143	1.395	1.305	1.641	1.178	1.485	1.355	1.773
	0.5	1.050	1.394	1.238	1.692	1.010	1.289	1.193	1.553	1.050	1.385	1.239	1.686
	1	1.142	1.464	1.320	1.753	1.101	1.361	1.264	1.608	1.138	1.453	1.318	1.745
	1.5	1.414	1.685	1.572	1.950	1.372	1.588	1.493	1.794	1.401	1.668	1.564	1.937
2	0	1.371	1.671	1.559	1.963	1.339	1.582	1.516	1.837	1.369	1.662	1.559	1.956
	0.5	1.250	1.573	1.448	1.876	1.217	1.480	1.411	1.751	1.249	1.565	1.449	1.870
	1	1.356	1.658	1.545	1.952	1.323	1.568	1.499	1.822	1.352	1.648	1.544	1.944
	1.5	1.646	1.903	1.818	2.174	1.612	1.818	1.751	2.035	1.636	1.888	1.811	2.163
a/b	$\bar{w}$	Multilayer hypar shells $V_{cn}^{*(k)} = 0.28$											
		0°				90°				0°/90°/0°			
1	0	0.934	1.204	1.106	1.463	0.990	1.339	1.169	1.629	0.936	1.209	1.106	1.465
	0.5	0.850	1.139	1.035	1.411	0.887	1.265	1.084	1.570	0.844	1.139	1.034	1.412
	1	0.981	1.241	1.146	1.494	1.041	1.377	1.213	1.662	0.985	1.248	1.147	1.497
	1.5	1.263	1.474	1.396	1.693	1.366	1.637	1.502	1.883	1.286	1.496	1.403	1.700
1.5	0	1.039	1.300	1.214	1.560	1.088	1.426	1.270	1.718	1.041	1.305	1.214	1.562
	0.5	0.958	1.236	1.145	1.508	0.991	1.353	1.188	1.658	0.953	1.236	1.144	1.508
	1	1.089	1.340	1.258	1.595	1.142	1.468	1.318	1.753	1.093	1.347	1.259	1.598
	1.5	1.373	1.579	1.512	1.802	1.467	1.733	1.610	1.982	1.394	1.601	1.519	1.809
2	0	1.249	1.496	1.435	1.763	1.289	1.607	1.482	1.904	1.250	1.500	1.436	1.765
	0.5	1.185	1.443	1.381	1.719	1.210	1.545	1.415	1.852	1.181	1.443	1.379	1.719
	1	1.335	1.568	1.515	1.828	1.377	1.679	1.563	1.967	1.338	1.574	1.515	1.830
	1.5	1.640	1.835	1.795	2.066	1.719	1.969	1.877	2.225	1.658	1.854	1.800	2.072
		90°/0°/90°				0°/90°/90°/0°				90°/0°/0°/90°			
1	0	0.988	1.334	1.169	1.627	0.941	1.222	1.108	1.474	0.984	1.323	1.168	1.620
	0.5	0.893	1.265	1.086	1.569	0.845	1.149	1.033	1.419	0.893	1.256	1.087	1.563
	1	1.037	1.371	1.212	1.659	0.991	1.261	1.150	1.506	1.032	1.359	1.211	1.651
	1.5	1.345	1.616	1.496	1.877	1.300	1.515	1.412	1.715	1.332	1.598	1.488	1.864
1.5	0	1.087	1.422	1.270	1.716	1.045	1.316	1.215	1.571	1.083	1.411	1.269	1.708
	0.5	0.996	1.354	1.190	1.657	0.954	1.245	1.143	1.515	0.996	1.345	1.191	1.651
	1	1.139	1.462	1.318	1.751	1.098	1.359	1.261	1.606	1.135	1.451	1.316	1.743
	1.5	1.448	1.713	1.604	1.976	1.407	1.619	1.527	1.823	1.436	1.696	1.596	1.964
2	0	1.288	1.603	1.482	1.902	1.254	1.510	1.437	1.772	1.285	1.594	1.482	1.895
	0.5	1.215	1.545	1.417	1.851	1.182	1.451	1.379	1.725	1.215	1.537	1.418	1.846
	1	1.374	1.674	1.563	1.965	1.342	1.584	1.517	1.837	1.371	1.664	1.561	1.958
	1.5	1.703	1.952	1.872	2.219	1.669	1.869	1.807	2.083	1.692	1.937	1.865	2.208

$(90°/0°/0°/90°)$, this difference decreases as r_1/a_1 increases. The two profiles being compared with each other, the SD effect in the V profile is less and the SD effect difference between the two profiles is maximum about (9%) for $(90°)$ and about (%9.35%) for $(90°/0°/0°/90°)$. As $\bar{w}$ increases, the V pattern effect on the NDNLF values in both shells at first increases about (1.6%) but later decreases about (2.4%) and this increase and decrease in CST gains more relevance for $(90°/0°/0°/90°)$ when $r_1/a_1 = 1$. When $\bar{w} = 1$ as r_1/a_1 passes from 2 to 3, in ML-SSs and ML-HSs, respectively, the V pattern effect decreases (0.72%) and (1.69%) for SDT and (1.1%) and (2.08%) for CST in the $(90°)$ layer order and (0.67%) and (1.79%) for SDT and

(1.02%) and (2.13%) for CST in the $(90°/0°/0°/90°)$ layer order. The V pattern effect difference between the two shells is maximum for SDT and CST, respectively, (3.36%) and (3.23%) in the $(90°)$ layer order and (3.77%) and (3.61%) in the $(90°/0°/0°/90°)$ layer order and this difference decreases as r_1/a_1 increases. For both shells and for both layer orders the SDT case decreases the V profile effect about (6.4%).

The variation of NDNLF/NDLF ratios of ML-SSs and ML-HSs with $\bar{w}$ for $r_1/a_1 = 1.5$, $a_1/a_2 = 1$, $a_1/h = 15$, $(m,n) = (1,1)$ and $V_{cn}^{*(k)} = 0.12$ is given in Fig. 7. As seen from Fig. 7a and b six different layer orders, $(0°)$, $(90°)$, $(0°/90°/0°)$, $(90°/0°/90°)$, $(0°/90°/90°/0°)$ and
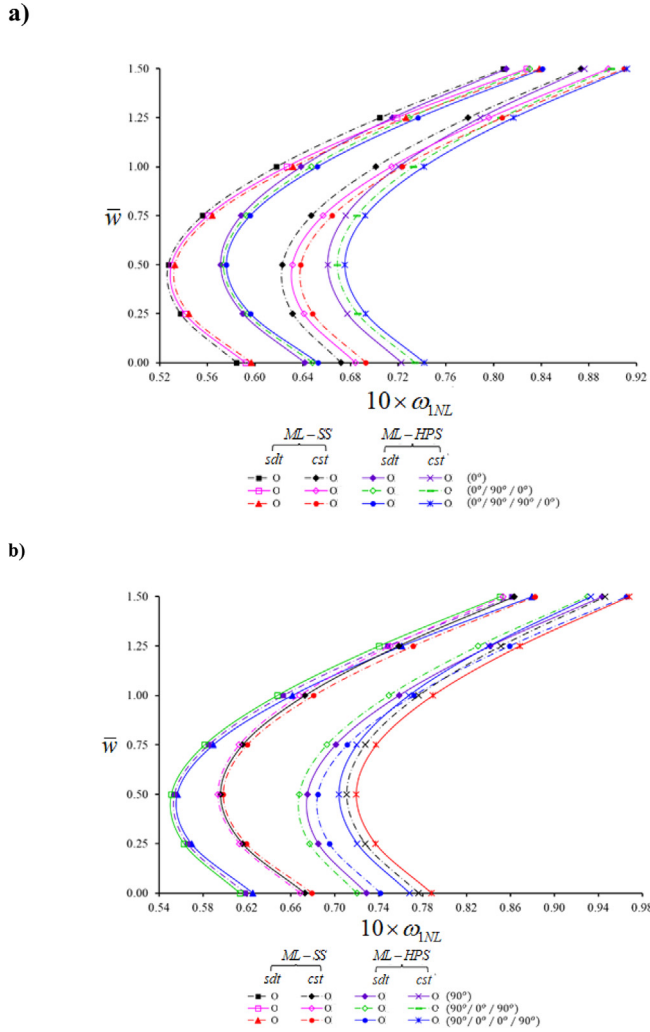
a)

b)

Fig. 5. $\bar{w}$ dependence of NDNLF values of ML-SSs and ML-HSs consisting of O type CNT patterned layers starting with (a) $(0°)$ and (b) $(90°)$ sequences.

$(90°/0°/0°/90°)$ and the V pattern are considered. As $\bar{w}$ increases, while the NDNLF/NDLF ratios decrease for all layer orders in both SDT and CST cases for $\bar{w} \leqslant 0.75$ in ML-SSs and for $\bar{w} \leqslant 0.5$ in ML-HSs, they increase in ML-SSs for $\bar{w} > 0.75$ and in ML-HSs for $\bar{w} > 0.5$. When the two shells are compared with each other, for all layer orders, the NDNLF/NDLF ratios are greater when $\bar{w} \geqslant 0.75$ for SDT and when $\bar{w} \geqslant 0.5$ for CST in ML-HSs. On the other hand, for all layer orders, while the maximum NDNLF/NDLF ratio is obtained in ML-SSs for CST and in ML-HSs for SDT when $\bar{w} = 1.25$ and the minimum ratio in ML-SSs for SDT when $\bar{w} = 0.75$ and in ML-HSs for SDT when $\bar{w} = 0.5$. In both shells for both SDT and CST cases the NDNLF/NDLF ratios in three and four layered shells are smaller when $(0°/90°/0°)$ and $(0°/90°/90°/0°)$ layer orders are compared with $(0°)$, whereas, larger when $(90°/0°/90°)$ and $(90°/0°/0°/90°)$ layer orders are compared with $(90°)$. As $\bar{w}$ increases, the SD effects on the NDNLF/NDLF ratios for $(0°)$, $(90°)$, $(0°/90°/0°)$, $(90°/0°/90°)$, $(0°/90°/90°/0°)$ and $(90°/0°/0°/90°)$, respectively, increase (4.65%), (6.16%), (5.09%), (5.69%), (5.35%) and (5.43%) in ML-SSs, when $\bar{w} \leqslant 0.75$, and (6%), (7.96%), (6.69%), (7.26%), (7.06%) and (6.9%) in ML-HSs when $\bar{w} \leqslant 0.5$. On the other hand, the same effects with the same conditions are decrease of (2.52%), (3.84%), (2.2%), (3.39%), (3.16%) and (3.18%) for ML-SSs, when $\bar{w} > 0.75$

and (4.42%), (6.76%), (5.54%), (6.1%), (5.89%) and (5.76%) for ML-HSs, when $\bar{w} > 0.5$. The maximum SD effect difference is (2.61%) for monolayer shell with the laminate $(90°)$ and minimum (1.01%) for monolayer shell with the laminate $(0°)$. In both shells, the SD effect obtained for $V_{cn}^{*(k)} = 0.12$ is greater than that for $V_{cn}^{*(k)} = 0.17$, whereas, smaller than the one for $V_{cn}^{*(k)} = 0.28$. The maximum SD effect differences between $V_{cn}^{*(k)} = 0.12$ and $V_{cn}^{*(k)} = 0.17$ are in ML-HSs and ML-SSs, respectively, (1.53%) and (1.18%) for $(90°)$ and (1.40%) and (1.08%) for $(90°/0°/90°)$. The maximum SD effect differences between $V_{cn}^{*(k)} = 0.12$ and $V_{cn}^{*(k)} = 0.28$ are in ML-HSs and ML-SSs, respectively, (1.48%) and (1.26%) for $(90°)$ and (1.38%) and (1.16%) for $(90°/0°/90°)$.

The variations of NDNLF/NDLF ratios in ML-SSs and ML-HSs with $\bar{w}$ for $r_1/a_1 = 1.5$, 2, 2.5, $a_1/a_2 = 0.5$, $a_1/h = 15$, $(m, n) = (1, 1)$ and $V_{cn}^{*(k)} = 0.17$ are presented by curves in graphical form in Fig. 8. As seen from Fig. 8a and b, two-layer orders, $(0°)$ and $(0°/90°/90°/0°)$, and two patterns, U and O, are being considered. In both shells, depending on the increase in $\bar{w}$ and the three values of r_1/a_1 the variation of NDNLF/NDLF ratios have different features. In ML-HSs for both layer orders, while they decrease in the range $\bar{w} \leqslant 0.5$, increase in the range $\bar{w} > 0.5$ when $r_1/a_1 < 2.5$ and while they decrease in the range $\bar{w} \leqslant 0.25$, increase in the range $\bar{w} > 0.25$ when $r_1/a_1 = 2.5$. On the other hand, in ML-SSs for both layer orders, while decreasing in the range $\bar{w} \leqslant 0.5$, increase in the range $\bar{w} > 0.5$ when $r_1/a_1 > 1.5$ and while decreasing in the range $\bar{w} \leqslant 0.75$, increase in the range $\bar{w} > 0.75$ when $r_1/a_1 = 1.5$. In both shells, NDNLF/NDLF ratios increase as R_1/a increases. When the two shells are compared with each other, in both profiles, the NDNLF/NDLF ratios are greater in ML-HSs for $r_1/a_1 > 1.5$ and in ML-SSs for $r_1/a_1 = 1.5$ with $\bar{w} = 0.25$. Moreover, in both shells and for both layer orders for $r_1/a_1 > 1.5$ and $\bar{w} > 1$ the NDNLF/NDLF ratios obtained for the O pattern are greater. As $\bar{w}$ increases O pattern effect on the NDNLF/NDLF ratios in both shells for $r_1/a_1 < 2$ at first increases and later decreases but for $r_1/a_1 > 2$ at first increases and later decreases but even later increases again. On the other hand, the maximum O pattern effects in both shells and for both layer orders are obtained for $r_1/a_1 = 2.5$ with $\bar{w} = 1.25$. In the end, the maximum O pattern effect for $(0°)$ and $(0°/90°/90°/0°)$, respectively, are in ML-SSs $(\%2.73)$ and $(\%2.59)$ while in ML-HSs $(\%4.44)$ and $(\%4.09)$.

The variation of NDNLF/NDLF ratios with $\bar{w}$ in ML-SSs for $n(m = 1) = 1$, 2, 3 and $m(n = 1) = 1$, 2, 3, $r_1/a_1 = 2$, $a_1/a_2 = 0.5$, $a_1/h = 15$ and $V_{cn}^{*(k)} = 0.28$ are presented in Fig. 9. As seen from Fig. 9a–d two different layer orders, $(0°)$ and $(0°/90°/90°/0°)$, and the U and X patterns are considered. Depending on the variation of $\bar{w}$ and the range of the number of waves, $n(m = 1)$ and $m(n = 1)$, the variation of NDNLF/NDLF ratios have different features. While the NDNLF/NDLF ratios increase as $n(m = 1)$ and $m(n = 1)$ pass from 1 to 2 and decrease as $n(m = 1)$ passes from 2 to 3 both for SDT and CST, as $n = 1$ and m passes from 2 to 3 they decrease for CST, but increase for SDT. The NDNLF/NDLF ratios increase, as $n(m = 1)$ changes, for $(n, m) = (1, 1)$ when $\bar{w}$ increases in the range $\bar{w} > 0.5$, for $(m, n) = (1, 3)$ in the range $\bar{w} > 0.25$ and for $(m, n) = (1, 2)$ with all $\bar{w}$, and as $m(n = 1)$ changes, for $(m, n) = (2, 1)$ and $(m, n) = (3, 1)$ for all values of $\bar{w}$. On the other hand, the values obtained for X pattern are smaller than those for SDT when $n(m = 1) \geqslant 2$ and $m(n = 1) \geqslant 2$, but vice versa in the range $\bar{w} < 1$, when $(n, m) = (1, 1)$. However, the NDNLF/NDLF obtained for SDT are larger when $n(m = 1) \geqslant 2$ and $m(n = 1) \geqslant 2$, but smaller in the range $\bar{w} < 1$ when $(n, m) = (1, 1)$. When the two layer orders are compared with each other for $(n, m) = (1, 1)$ in the range $\bar{w} \leqslant 0.75$ the values obtained for $(0°/90°/90°/0°)$ layer order are less than those for $(0°)$ shell and
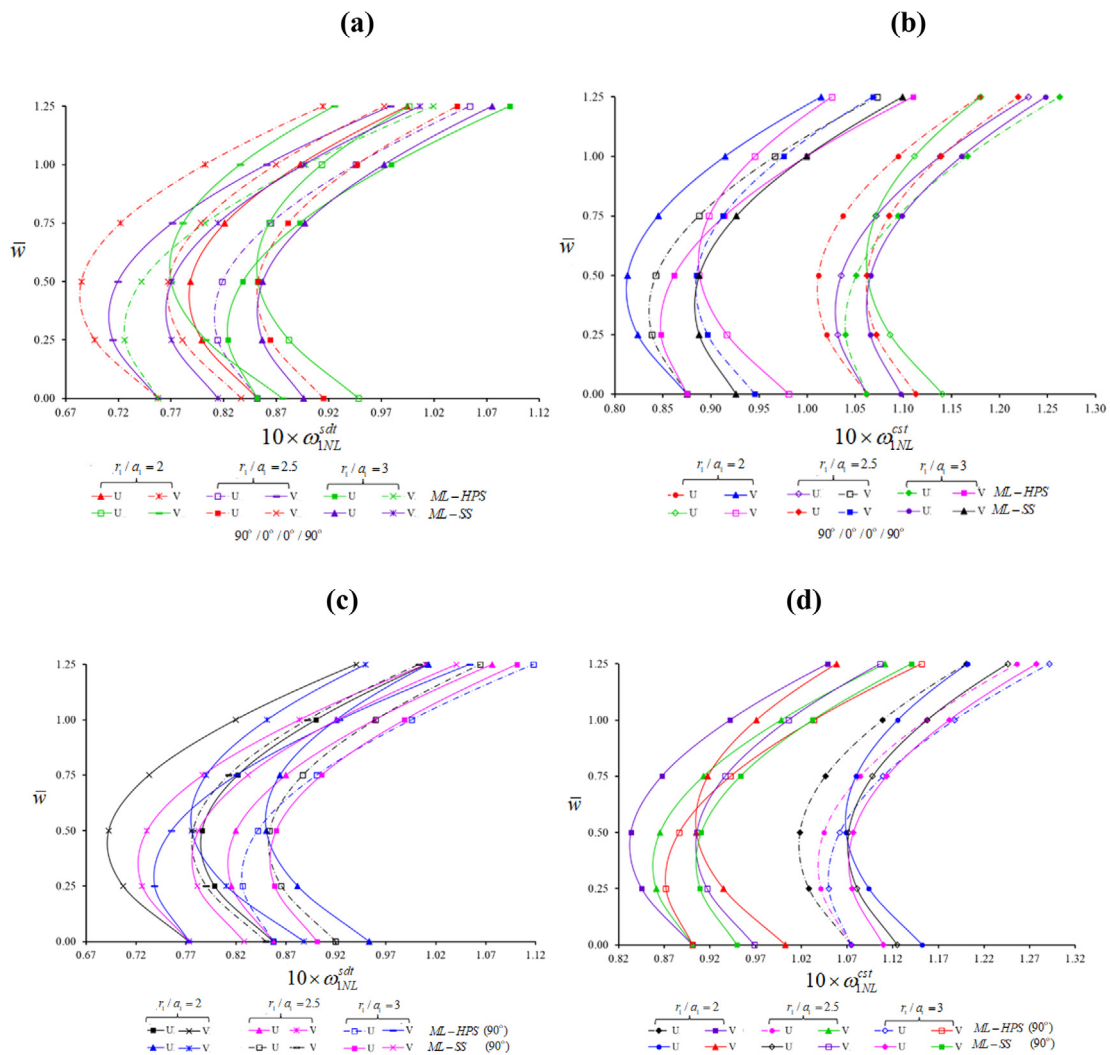
(a)

(b)

(c)

(d)

Fig. 6. $\bar{w}$ dependence of NDNLF values of ML-SSs and ML-HSs consisting of U and V type CNT patterned layers with the arrangements $(90°/0°/0°/90°)$ within (a) SDT and (b) CST, and for single layer $(90°)$ within (c) SDT and (d) CST.

outside that range and if only one of the wave numbers is equal to and the other larger than one, it is vice versa. While the NDNLF/NDLF ratios increase as n ($m = 1$) and m ($n = 1$) pass from 1 to 2 and decrease as $m = 1$ and n pass from 2 to 3 both for SDT and CST, as $n = 1$ and m passes from 2 to 3 they decrease for CST, but increase for SDT. The NDNLF/NDLF ratios increase, as $m = 1$ and n changes, for $(m, n) = (1, 1)$ when $\bar{w}$ increases in the range $\bar{w} > 0.5$, for $(m, n) = (1, 3)$ in the range $\bar{w} > 0.25$ and for $(m, n) = (1, 3)$ with all $\bar{w}$, and as $n = 1$ and m changes, for $(m, n) = (2, 1)$ and $(m, n) = (3, 1)$ for all values of $\bar{w}$. As $\bar{w}$ increases, the SD effect on NDNLF/NDLF increases steadily when $n(m = 1) \geqslant 2$ and $m(n = 1) \geqslant 2$, but decreases, and then increases again, in that order, when $n = m = 1$. As the wave number $n(m = 1)$ passes from 1 to 2, the SD effect increases, whereas, when the wave number passes from 2 to 3 it decreases. As the wave number $m(n = 1)$ passes from 1 to 2 and $n(m = 1)$ passes from 2 to 3, the SD effect increases in the range $\bar{w} \leqslant 1$. For example, for $n(m = 1) = 2$ as $\bar{w}$ increases from 0 to 1.5 about (13%) and (14%) and for $m(n = 1) = 2$ about (57%) and (60%) increases take place, respectively, in $(0°)$ and $(0°/90°/90°/0°)$ layer orders. When $\bar{w} = 1$ as $n(m = 1)$ passes from 1 to 3 for $(0°)$ and $(0°/90°/90°/0°)$ layer orders, respectively, at first increases of about (8%) and (9%) and later decreases of about (3.6%) and (4%) and as $m(n = 1)$ passes from 1 to 3

increases of about (43%) and (45%) take place. The SD effect differences between the two-layer orders are about (3.5%) for $m(n = 1) = 2$ and about (1.0%) for all other wave numbers. As $\bar{w}$ increases, the X pattern effect on NDNLF/NDLF increases for $n(m = 1) \geqslant 2$ and $m(n = 1) \geqslant 2$, whereas, increases, decreases, and increases again for $n = m = 1$. As the wave number $n(m = 1)$ passes from 1 to 2 effect of X pattern increases, but as $n(m = 1)$ passes from 2 to 3 it decreases. As the wave number $m(n = 1)$ passes from 1 to 3, the X pattern effect increases. As $\bar{w}$ increases, the maximum X pattern effect change is (9.8%) for $n(m = 1)$ and (14.09%) for $m(n = 1)$, both being obtained for $(0°/90°/90°/0°)$ layer order and as the wave numbers increase, the maximum X pattern effect change for $n(m = 1)$ is (7%) and for $m(n = 1)$ is (13.14%), which are also obtained for the same layer order.

6. Conclusions

In this article, the vibration of multilayer shell-type structural elements with double curvature consisting of CNT patterned layers at finite deflection is investigated within different shell theories. The FSDT has been generalized for the vibration problem of multilayer shell-type structural elements with double curvature consisting of CNT patterned layers for the first time. After creating the models of
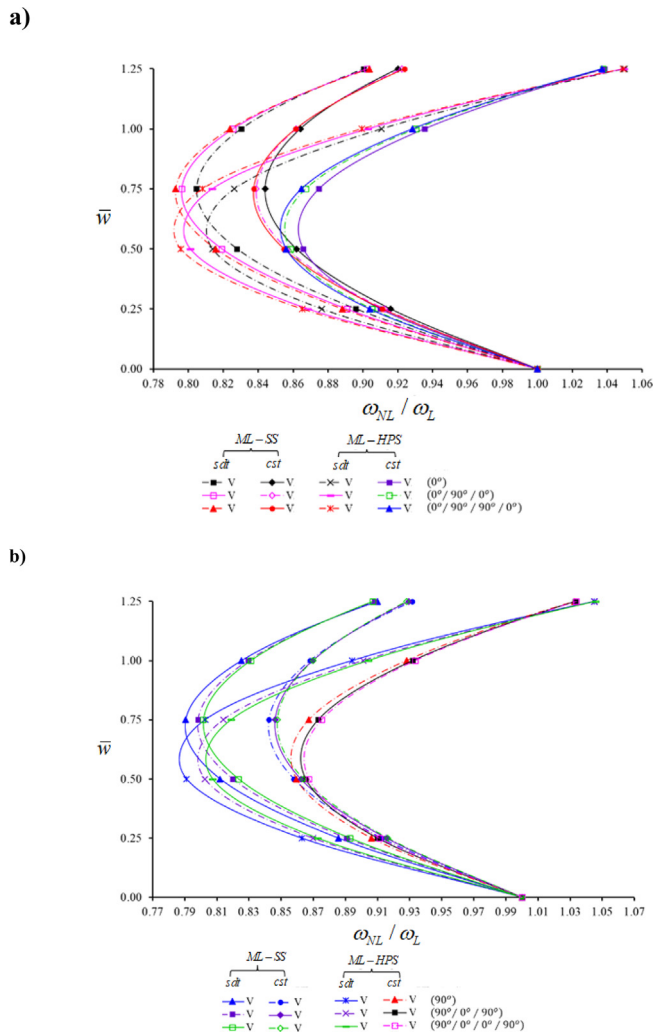
a)

b)

Fig. 7. $\bar{w}$ dependence of NDNLF values of ML-SSs and ML-HSs consisting of V type CNT patterned layers starting with sequences (a) (0°) and (b) (90°) within SDT and CST.

a)

b)

Fig. 8. $\bar{w}$ dependence of NL-FVF/L-FV ratio of ML-SSs and ML-HSs consisting of U and O type CNT patterned layers with the arrangements (a)(0°/90°/90°/0°) and for (b) monolayer (0°) within SDT for different r_1/a_1.

multilayer shell-type structural elements with double curvature consisting of CNT patterned layers, basic relations and dynamic equations in finite deflections are derived. Then, by applying Galerkin and semi-inverse perturbation methods to motion equations of multilayer shell-type structural elements with double curvature consisting of CNT patterned layers based on Airy stress function, deflection function and rotation angle functions frequency-amplitude relationship is obtained. From these formulas, the expressions for nonlinear frequencies of multilayer spherical and hyperbolic-paraboloid shells, rectangular plate and cylindrical panels patterned by CNTs within shear deformation and classical shell theories are obtained in special cases. The safety of the proposed formulation has been confirmed by comparison with the results available in the literature. The effects of CNT patterns in layers, volume fractions, sequence and number of layers on nonlinear frequency are discussed in detail in the framework of SDT and CST, and the changes of these effects in terms of quantity and quality are presented.

Author Statement

We confirm that, this is an original paper, has not been submitted elsewhere for publication and has not been published elsewhere.
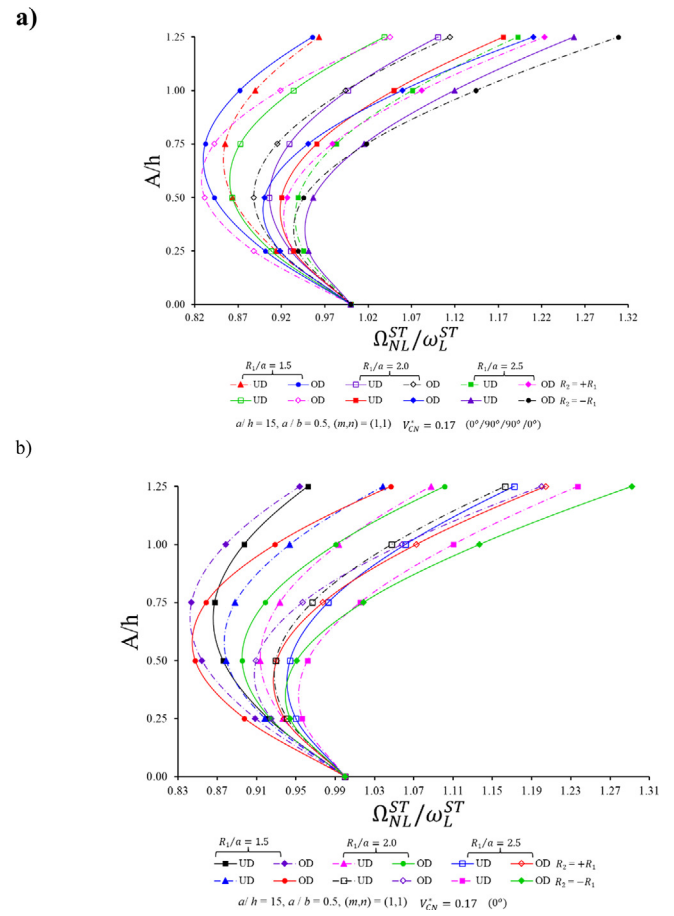
Funding Source

CRediT authorship contribution statement

M. Avey: Conceptualization, Methodology, Funding acquisition, Formal analysis, Writing - review & editing. **N. Fantuzzi:** Methodology, Formal analysis, Investigation, Writing - review & editing. **A.H. Sofiyev:** Formal analysis, Writing - original draft. **N. Kuruoglu:** Writing - review & editing.

Declaration of Competing Interest

The authors declare that they have no known competing financial interests or personal relationships that could have appeared to influence the work reported in this paper.

Appendix A

B_{ij}, $S_{ij}(i = 1, 2, ..., 4, j = 1, 2, ..., 5)$ and $I_k(k = 3, 4)$ are defined as:
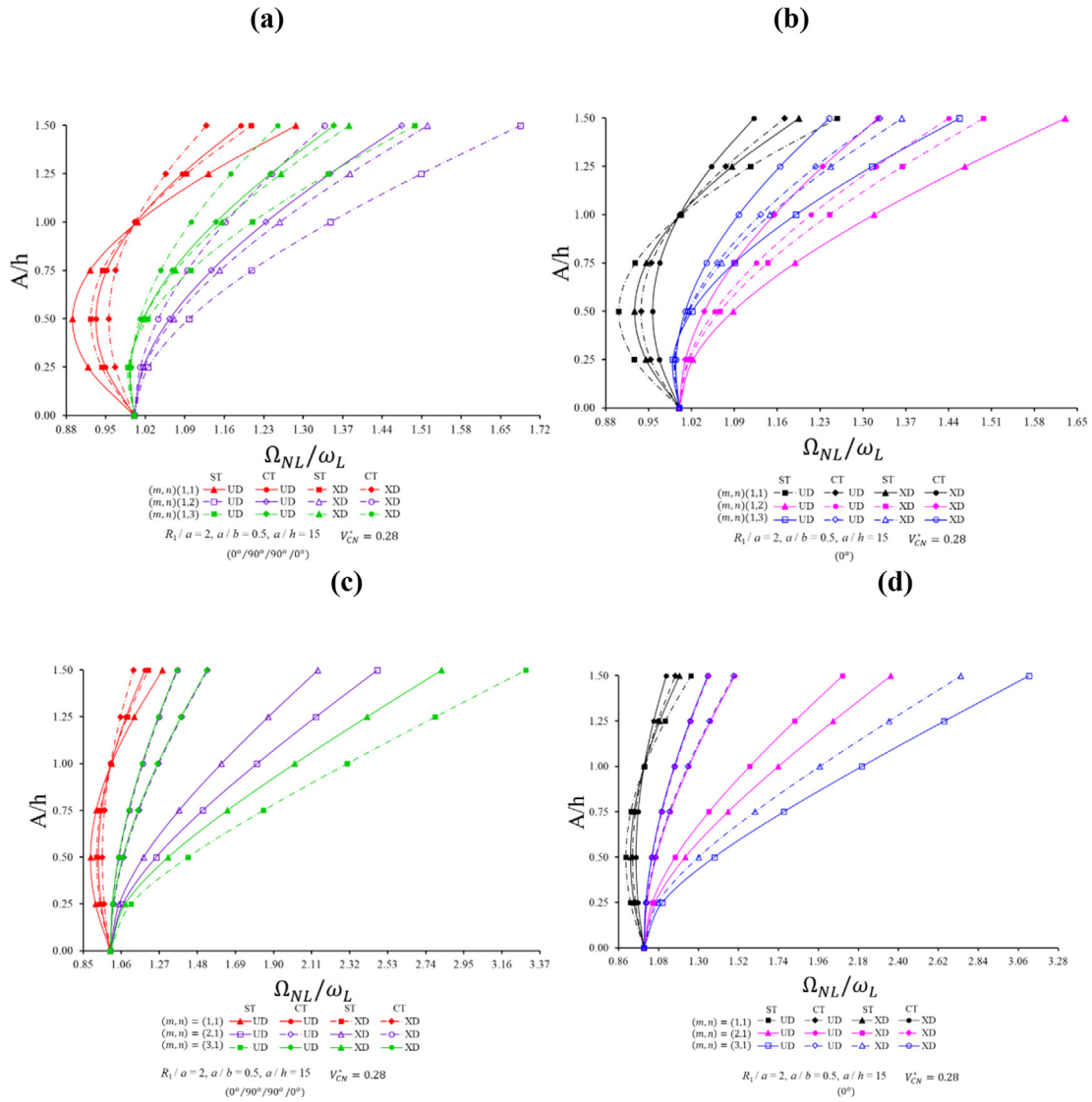
(a)

(b)

(c)

(d)

Fig. 9. $\bar{w}$ dependence of NDNLF/NDLF ratio of ML-SSs and ML-HSs consisting of UD and VD type CNT patterned layers with the arrangements $(0°/90°/90°/0°)$ within (a) SDT and (b) CST, and for single layer $0°$ within (c) SDT and (d) CST.

$$S_{11} = A^1_{11}B_{11} + A^1_{12}B_{21}, \ S_{12} = A^1_{11}B_{12} + A^1_{12}B_{11},$$
$$S_{13} = A^1_{11}B_{13} + A^1_{12}B_{23} + A^2_{11}, \ S_{14} = A^1_{11}B_{14} + A^1_{12}B_{24} + A^2_{12},$$
$$S_{15} = A^1_{11}B_{15} + A^1_{12}B_{25} + A^1_{15}, \ S_{18} = A^1_{11}B_{18} + A^1_{12}B_{28} + A^1_{18},$$
$$S_{21} = A^1_{21}B_{11} + A^1_{22}B_{21}, \ S_{22} = A^1_{21}B_{12} + A^1_{22}B_{22},$$
$$S_{23} = A^1_{21}B_{13} + A^1_{22}B_{23} + A^2_{21}, \ S_{24} = A^1_{21}B_{14} + A^1_{22}B_{24} + A^2_{22},$$
$$S_{25} = A^1_{21}B_{15} + A^1_{22}B_{25} + A^1_{25}, \ S_{28} = A^1_{21}B_{18} + A^1_{22}B_{28} + A^1_{28},$$
$$S_{31} = A^1_{66}B_{35}, \ \ S_{32} = A^1_{66}B_{32} + 2A^2_{66}$$
$$S_{35} = A^1_{35} - A^1_{66}B_{35}, \ S_{38} = A^1_{38} - A^1_{66}B_{38},$$
$$I_k = \sum_{k=1}^n \int_{-h/2+(k-1)h/N}^{-h/2+kh/N} \frac{df^{(k)}_{jx_3}}{dx_3} dx_3, (k = 3,4) \tag{A1}$$

where

$$B_{11} = \frac{A^0_{22}}{\Lambda}, \ \ B_{12} = -\frac{A^0_{12}}{\Lambda}, \ \ B_{13} = \frac{A^0_{12}A^1_{21}-A^1_{11}A^0_{22}}{\Lambda}, \ \ B_{14} = \frac{A^0_{12}A^1_{22}-A^1_{12}A^0_{22}}{\Lambda},$$
$$B_{15} = \frac{A^0_{25}A^0_{12}-A^0_{15}A^0_{22}}{\Lambda}, B_{18} = \frac{A^0_{28}A^0_{12}-A^0_{18}A^0_{22}}{\Lambda}, \ B_{21} = -\frac{A^0_{21}}{\Lambda}, \ \ B_{22} = \frac{A^0_{11}}{\Lambda},$$
$$B_{23} = \frac{A^1_{11}A^0_{21}-A^1_{21}A^0_{11}}{\Lambda}, \ \ B_{24} = \frac{A^1_{12}A^0_{21}-A^1_{22}A^0_{11}}{\Lambda}, \ \ B_{25} = \frac{A^0_{15}A^0_{21}-A^0_{25}A^0_{11}}{\Lambda},$$
$$B_{28} = \frac{A^0_{18}A^0_{21}-A^0_{28}A^0_{11}}{\Lambda}, \ \ B_{31} = \frac{1}{A^0_{66}}, \ \ B_{32} = -\frac{2A^1_{66}}{A^0_{66}}, \ \ B_{35} = \frac{A^0_{35}}{A^0_{66}}, \ B_{38} = \frac{A^0_{38}}{A^0_{66}},$$
$$\Lambda = A^0_{11}A^0_{22} - A^0_{12}A^0_{21}, \tag{A2}$$

in which the following symbols are used:

$$A^{k_1}_{11} = \sum_{k=1}^n \int_{-h/2+(k-1)h/N}^{-h/2+kh/N} Q^{(k)}_{11\bar{x}_3} x_3^{k_1} dx_3,$$
$$A^{k_1}_{12} = \sum_{k=1}^n \int_{-h/2+(k-1)h/N}^{-h/2+kh/N} Q^{(k)}_{12\bar{x}_3} x_3^{k_1} dx_3,$$
$$A^{k_1}_{21} = \sum_{k=1}^n \int_{-h/2+(k-1)h/N}^{-h/2+kh/N} Q^{(k)}_{21\bar{x}_3} x_3^{k_1} dx_3,$$
$$A^{k_1}_{22} = \sum_{k=1}^n \int_{-h/2+(k-1)h/N}^{-h/2+kh/N} Q^{(k)}_{22\bar{x}_3} x_3^{k_1} dx_3,$$
$$A^{k_1}_{66} = \sum_{k=1}^n \int_{-h/2+(k-1)h/N}^{-h/2+kh/N} G^{(k)}_{12\bar{x}_3} x_3^{k_1} dx_3,$$
$$A^{k_2}_{15} = \sum_{k=1}^n \int_{-h/2+(k-1)h/N}^{-h/2+kh/N} Q^{(k)}_{11\bar{x}_3} I^{(k)}_{1x_3} x_3^{k_2} dx_3,$$
$$A^{k_2}_{18} = \sum_{k=1}^n \int_{-h/2+(k-1)h/N}^{-h/2+kh/N} Q^{(k)}_{12\bar{x}_3} I^{(k)}_{2x_3} x_3^{k_2} dx_3, \tag{A3}$$
$$A^{k_2}_{25} = \sum_{k=1}^n \int_{-h/2+(k-1)h/N}^{-h/2+kh/N} Q^{(k)}_{21\bar{x}_3} I^{(k)}_{1x_3} x_3^{k_2} dx_3,$$
$$A^{k_2}_{28} = \sum_{k=1}^n \int_{-h/2+(k-1)h/N}^{-h/2+kh/N} Q^{(k)}_{22\bar{x}_3} I^{(k)}_{2x_3} x_3^{k_2} dx_3,$$
$$A^{k_2}_{35} = \sum_{k=1}^n \int_{-h/2+(k-1)h/N}^{-h/2+kh/N} Q^{(k)}_{66\bar{x}_3} I^{(k)}_{1x_3} x_3^{k_2} dx_3,$$
$$A^{k_2}_{35} = \sum_{k=1}^n \int_{-h/2+(k-1)h/N}^{-h/2+kh/N} Q^{(k)}_{66\bar{x}_3} I^{(k)}_{2x_3} x_3^{k_2} dx_3, \ \ (k_1 = 0, 1, 2; \ k_2 = 0, 1).$$

Appendix B

The parameter μ_{ij} are defined as

$$\mu_{11} = \Delta_3 h\big[(S_{11} - S_{31})\lambda_1^2\lambda_2^2 + S_{12}\lambda_1^4\big]\alpha_{11} - S_{13}\lambda_1^4 - (S_{14} + S_{32})\lambda_1^2\lambda_2^2,$$

$$\mu_{11}^{NL} = -hS_{12}\frac{64\Delta_1}{3a_1a_2}\frac{\lambda_1^3}{\lambda_2}\big[1 - (-1)^m - (-1)^n + (-1)^{m+n}\big], \quad \mu_{11}^{\tau} = -\rho_1 h^3 \lambda_1^2,$$

$$\mu_{12} = (S_{15}\lambda_2^3 + S_{35}\lambda_1 + I_3)\lambda_1, \quad \mu_{12}^{\tau} = \rho_2 h^3 \lambda_1, \quad \mu_{13} = (S_{18} + S_{38})\lambda_1^2\lambda_2,$$

$$\mu_{21} = \big\{\alpha_{11}h\Delta_3\big[S_{21}\lambda_2^2 + (S_{22} - S_{31})\lambda_1^2\big] - (S_{32} + S_{23})\lambda_1^2 - S_{24}\lambda_2^2\big\}\lambda_2^2,$$

$$\mu_{21}^{NL} = -S_{21}h\frac{64\Delta_2}{3a_1^2}\frac{\lambda_2^3}{\lambda_1}\big(1 - (-1)^m - (-1)^n + (-1)^{m+n}\big), \quad \mu_{21}^{\tau} = -\rho_1 h^3 \lambda_2^2,$$

$$\mu_{22} = (S_{25} + S_{35})\lambda_1\lambda_2^2, \quad \mu_{23} = \big(S_{28}\lambda_2^2 + S_{38}\lambda_1^2 + I_4\big)\lambda_2, \quad \mu_{23}^{\tau} = \rho_3 h^3 \lambda_2,$$

$$\mu_{31} = h\Delta_3\left(\frac{\lambda_1^2}{r_2} + \frac{\lambda_2^2}{r_1}\right)\alpha_{11}, \quad \mu_{32} = 2\lambda_1^2\lambda_2^2 h(\Delta_1 + \Delta_2),$$

$$\mu_{31}^{NL} = -\frac{8h}{3a_1a_2}\left[2\left(\frac{\Delta_1}{r_2}\frac{\lambda_1}{\lambda_2} + \frac{\Delta_2}{r_1}\frac{\lambda_2}{\lambda_1}\right) + \lambda_1\lambda_2\alpha_{11}\Delta_3\right]\big[1 - (-1)^m - (-1)^n + (-1)^{m+n}\big],$$

$$\mu_{33} = I_3\lambda_1, \quad \mu_{34} = I_4\lambda_2 \tag{B1}$$

where

$$\Delta_1 = \frac{\lambda_2^2}{32\lambda_1^2\alpha_3}, \quad \Delta_2 = \frac{\lambda_1^2}{32\lambda_2^2\alpha_1}, \quad \Delta_3 = \frac{1}{\alpha_1\lambda_2^4 + \alpha_2\lambda_2^2\lambda_1^2 + \alpha_3\lambda_1^4} \tag{B2}$$

References

[1] Ambartsumian SA. Theory of anisotropic shells. NASA, TT F-118 1964.

[2] Librescu L, Frederick KAA, DA.. Shear deformable theory of laminated composite shallow shell-type panels and their response analysis. 1. free-vibration and buckling. Acta Mech 1989;76(1–2):1–33.

[3] Xu CS, Chia CY. Nonlinear-analysis of unsymmetrically laminated moderately thick shallow spherical-shells. Int J Non-Lin Mech 1994;29(2):247–59.

[4] Wang J, Schweizerhof K. The fundamental-solutions of moderately thick laminated anisotropic shallow shells. Int J Eng Sci 1995;33(7):995–1004.

[5] Reddy JN. Mechanics of laminated composite plates and shells theory and analysis. CRC Press; 2004.

[6] Viola E, Tornabene F, Fantuzzi N. General higher-order shear deformation theories for the free vibration analysis of completely doubly-curved laminated shells and panels. Compos Struct 2013;95:639–66.

[7] Wang YQ. Nonlinear vibration of a rotating laminated composite circular cylindrical shell: traveling wave vibration. Nonlinear Dyn 2014;77(4):1693–707.

[8] Amabili M. A new third-order shear deformation theory with non-linearities in shear for static and dynamic analysis of laminated doubly curved shells. Compos Struct 2015;128:260–73.

[9] Tornabene F, Fantuzzi N, Bacciocchi M. On the mechanics of laminated doubly-curved shells subjected to point and line loads. Int J Eng Sci 2017;109:288–304.

[10] Sofiyev AH. Application of the first order shear deformation theory to the solution of free vibration problem for laminated conical shells. Compos Struct 2018;188:340–6.

[11] Kurpa L, Timchenko G, Osetrov A, Shmatko T. Nonlinear vibration analysis of laminated shallow shells with clamped cutouts by the R-functions method. Nonlin Dyn 2018;93(1):133–47.

[12] Li C, Li P, Zhong B, Wen B. Geometrically nonlinear vibration of laminated composite cylindrical thin shells with non-continuous elastic boundary conditions. Nonlin Dyn 2019;95(3):1903–21.

[13] Huang S, Qiao P. A new semi-analytical method for nonlinear stability analysis of stiffened laminated doubly-curved shallow shells. Compos Struct 2020;251:112526. https://doi.org/10.1016/j.compstruct.2020.112526.

[14] Shahmohammadi MA, Abdollahi P, Salehipour H. Geometrically nonlinear analysis of doubly curved imperfect shallow shells made of functionally graded carbon nanotube reinforced composite (FG_CNTRC). Mech Based Des Struct Mach 2020. https://doi.org/10.1080/15397734. 20 20.1822182.

[15] Zhai Y, Ma J, Liang S. Dynamics properties of multi-layered composite sandwich doubly-curved shells. Compos Struct 2021;256:113142. https://doi.org/10.1016/j.compstruct.2020.113142.

[16] Iijima S. Helical microtubules of graphitic carbon. Nature 1991;354(6348):56–8.

[17] Lu JP. Elastic properties of carbon nanotubes and nanoropes. Phys Rev Let 1997;79(7):1297–300.

[18] Park SH, Bae J. Polymer composite containing carbon nanotubes and their applications. Rec Patents Nanotech 2017;11(2):109–15.

[19] Fantuzzi N, Bacciocchi M, Agnelli J, Benedetti D. Three-phase homogenization procedure for woven fabric composites reinforced by carbon nanotubes in thermal environment. Compos Struct 2020;254:112840. https://doi.org/10.1016/j.compstruct.2020.112840.

[20] Shen HS, Xiang Y. Nonlinear vibration of nanotube-reinforced composite cylindrical shells in thermal environments. Comp Meth Appl Mech Eng 2012;213:196–205.

[21] Pouresmaeeli S, Fazelzadeh SA. Frequency analysis of doubly curved functionally graded carbon nanotube-reinforced composite panels. Acta Mech 2016;227(10):2765–94.

[22] Nguyen PD, Quang VD, Anh VTT, Duc ND. Nonlinear vibration of carbon nanotube reinforced composite truncated conical shells in thermal environment. Int J Struct Stab Dyn 2019;19(12):1950158. https://doi.org/10.1142/S021945541950158X.

[23] Avey M, Yusufoglu E. On the solution of large-amplitude vibration of carbon nanotube-based doubly-curved shells. Math Meth Appl Sci 2020;1–13. https://doi.org/10.1002/mma.6820.

[24] Mahesh V. Nonlinear deflection of carbon nanotube reinforced multiphase magneto-electro-elastic plates in thermal environment considering pyrocoupling effects. Math Meth Appl Sci 2020. https://doi.org/10.1002/mma.6858.

[25] Zghal S, Frikha A, Dammak F. Large deflection responses-based geometrical nonlinearity of nanocomposite structures reinforced with carbon nanotubes. Appl Math Mech (English Edition) 2020;41:1227–50.

[26] Lee S-Y. Dynamic stability and nonlinear transient behaviors of CNT-reinforced fiber/polymer composite cylindrical panels with delamination around a cutout. Nonlin Dyn 2020;99(4):2551–69.

[27] Sofiyev AH, Avey M, Kuruoglu N. An approach to the solution of nonlinear forced vibration problem of structural systems reinforced with advanced materials in the presence of viscous damping. Mech Syst Signal Proces 2021;161:107991. https://doi.org/10.1016/j.ymssp.2021.107991.

[28] Tran HQ, Vu VT, Tran MT, Nguyen-Tri P. A new four-variable refined plate theory for static analysis of smart laminated functionally graded carbon nanotube reinforced composite plates. Mech Mater 2020;142:103294. https://doi.org/10.1016/j.mechmat.2019.103294.

[29] Mahmoodi MJ, Rajabi Y, Khodaiepour B. Electro-thermo-mechanical responses of laminated smart nanocomposite moderately thick plates containing carbon nanotube – A multi-scale modeling. Mech Mater 2020;141:103247. https://doi.org/10.1016/j.mechmat.2019.103247.

[30] Awrejcewicz J, Krysko VA. Nonlinear coupled problems in dynamics of shells. Int J Eng Sci 2003;41(6):587–607.

[31] Alijani F, Amabili M, Karagiozis K, Bakhtiari-Nejad F. Non-linear vibrations of functionally graded doubly curved shallow shells. J Sound Vib 2011;330(7):1432–54.

[32] Huy Bich D, Dinh Duc N, Quoc Quan T. Nonlinear vibration of imperfect eccentrically stiffened functionally graded double curved shallow shells resting on elastic foundation using the first order shear deformation theory. Int J Mech Sci 2014;80:16–28.

[33] Sheng GG, Wang X, Fu G, Hu H. The nonlinear vibrations of functionally graded cylindrical shells surrounded by an elastic foundation. Nonlin. Dyn. 2014;78:1421–34.

[34] Awrejcewicz J, Kurpa L, Shmatko T. Investigating geometrically nonlinear vibrations of laminated shallow shells with layers of variable thickness via the R-functions theory. Compos Struct 2015;125:575–85.

[35] Sheng GG, Wang X. The non-linear vibrations of rotating functionally graded cylindrical shells. Nonlin Dyn 2017;87(2):1095–109.

[36] Awrejcewicz J, Kurpa L, Shmatko T. Linear and nonlinear free vibration analysis of laminated functionally graded shallow shells with complex plan form and different boundary conditions. Int J Non-Lin Mech 2018;107:161–9.

[37] Tocci Monaco G, Fantuzzi N, Fabbrocino F, Luciano R. Hygro-thermal vibrations and buckling of laminated nanoplates via nonlocal strain gradient theory. Compos Struct 2021;262:113337. https://doi.org/10.1016/j.compstruct.2020.113337.

[38] Volmir AS. The nonlinear dynamics of plates and shells. Moscow: Sci. Edit; 1972.

[39] Nayfeh AH, Mook DT. Nonlinear oscillations. New York: Wiley; 1979.

[40] He J-H. Variational principles for some nonlinear partial differential equations with variable coefficients. Chaos Solutions Fractals 2004;19(4):847–51.

[41] Smirnov VV, Manevitch LI. Semi-inverse method in nonlinear mechanics: application to couple shell- and beam-type oscillations of single-walled carbon nanotubes. Nonlin Dyn 2018;93(1):205–18.